



**SCREENING DRUG LIBRARIES TO DISCOVER
VIRUS-DIRECTED OR HOST-DIRECTED
THERAPY FOR EV-A71 INFECTION**

BY

MISS NATTINEE LOCHAIYAKUN

**A THESIS SUBMITTED IN PARTIAL FULFILLMENT OF
THE REQUIREMENTS FOR THE DEGREE OF
MASTER OF SCIENCE (BIOMEDICAL SCIENCES)
GRADUATE PROGRAM IN BIOMEDICAL SCIENCES
FACULTY OF ALLIED HEALTH SCIENCES
THAMMASAT UNIVERSITY
ACADEMIC YEAR 2023**

**SCREENING DRUG LIBRARIES TO DISCOVER
VIRUS-DIRECTED OR HOST-DIRECTED
THERAPY FOR EV-A71 INFECTION**

BY

MISS NATTINEE LOCHAIYAKUN

**A THESIS SUBMITTED IN PARTIAL FULFILLMENT OF
THE REQUIREMENTS FOR THE DEGREE OF
MASTER OF SCIENCE (BIOMEDICAL SCIENCES)
GRADUATE PROGRAM IN BIOMEDICAL SCIENCES
FACULTY OF ALLIED HEALTH SCIENCES
THAMMASAT UNIVERSITY
ACADEMIC YEAR 2023**

THAMMASAT UNIVERSITY
FACULTY OF ALLIED HEALTH SCIENCES

THESIS

BY

MISS NATTINEE LOCHAIYAKUN

ENTITLED

SCREENING DRUG LIBRARIES TO DISCOVER
VIRUS-DIRECTED OR HOST-DIRECTED THERAPY FOR EV-A71 INFECTION

was approved as partial fulfillment of the requirements for
the degree of Master of Science

on June 21st, 2024

Chairman

Kantaphon G.

(Kantaphon (Kittirat) Glab-ampai, Ph.D.)

Member and Advisor

Jeeraphong T.

(Assoc. Prof. Jeeraphong Thanongsaksrikul, Ph.D.)

Member and Co-advisor

Potjanee S.

(Assoc. Prof. Potjanee Srimanote, Ph.D.)

Member and Co-advisor

Onruedee K.

(Asst. Prof. Onruedee Khantisitthiporn, Ph.D.)

Dean

Plaiwan Suttanon

(Assoc. Prof. Plaiwan Suttanon, Ph.D.)

Thesis Title	SCREENING DRUG LIBRARIES TO DISCOVER VIRUS-DIRECTED OR HOST- DIRECTED THERAPY FOR EV-A71 INFECTION
Author	Miss Nattinee Lochaiyakun
Degree	Master of Science (Biomedical Sciences)
Major Field/Faculty/University	Graduate Program in Biomedical Sciences Faculty of Allied Health Sciences Thammasat University
Thesis Advisor	Assoc. Prof. Jeerapong Thanongsaksrikul, Ph.D
Thesis Co-advisor	Assoc. Prof. Potjanee Srimanote, Ph.D.
Thesis Co-advisor	Asst. Prof. Onruedee Khantisitthiporn, Ph.D.
Academic Year	2023

ABSTRACT

The MMV Pandemic Response Box drug library contains a chemically and pharmacologically diverse mixture of early-stage, emerging anti-infective scaffolds, and mature compounds currently undergoing clinical development. It is an assembly of 153 antiviral agents, 201 antibacterial, and 46 antifungal compounds. In this thesis, only 153 antiviral agents were used for screening enterovirus A71 (EV-A71) inhibitors. It was hypothesized that the antiviral agents contained in the Pandemic Response Box might have compounds that bind and interfere with target molecules or cellular pathways that are conserved or shared among the closely related viruses with the EV-A71. This thesis aimed to screen antiviral agents included in the Pandemic Response Box for repurposing to anti-EV-A71 activity and investigate the inhibitory effects of the compounds on viral replication. Seven compounds were found to have negligible cytotoxicity cells and the ability to rescue the infected cells. The hit compounds were verified for anti-EV-A71 activity by virus reduction assays for viral RNA copy numbers, viral protein synthesis, and mature particle production using qRT-PCR, Western blot analysis, and CCID₅₀ assay, respectively. Some of the hit compounds could reduce EV-A71 genome replication and protein synthesis. It was found that D-

D7 (2-pyridone-containing human rhinovirus 3C protease inhibitor) exhibited the highest anti-EV-A71 activity. The 2-pyridone-containing human rhinovirus 3C protease inhibitor could be repurposed as an anti-EV-A71 agent by targeting a conserved substrate-binding motif of the enzyme.

Keywords: Enterovirus; Enterovirus A71; Hand-foot-mouth disease; Antivirus drugs; Repurposed drugs



ACKNOWLEDGEMENTS

I would like to thank all the important persons who gave me support and suggestions that helped me to carry on this thesis and laboratory work.

Firstly, I would like to thank the most important person my advisor Assoc. Prof. Jeeraphong Thanongsaksrikul for his advice, teaching, encouragement, scholarship, motivation, warm kindness, and mercy during my study and thesis preparation. He always helped and supported me in everything that made the thesis so well. Thank you for spending the time and recommendations on this dissertation.

I am thankful to my co-advisors, Assoc. Prof. Potjanee Srimanote, Asst. Prof. Pongsri Tongtawe, Asst. Prof. Onruedee Khantisitthiporn for their kind laboratory support and valuable suggestions in this work. I would like to thank P’Kob and all laboratory staff for providing advice, encouragement, smiles, and laughter, without them I would not have been able to complete this research. They always cheered me up and made me feel comfortable.

I acknowledge financial support from the Thailand Science Research and Innovation Fundamental Fund fiscal year 2023 and the Thammasat University Research Unit in Molecular Pathogenesis and Immunology of Infectious Disease.

Nattinee Lochaiyakun

TABLE OF CONTENTS

	page
ABSTRACT	(1)
ACKNOWLEDGEMENTS	(3)
TABLE OF CONTENTS	(4)
LIST OF TABLES	(8)
LIST OF FIGURES	(9)
LIST OF ABBREVIATIONS	(10)
CHAPTER 1 INTRODUCTION	1
CHAPTER 2 LITERATURE REVIEW	3
2.1 Enterovirus A71 (EV-A71)	3
2.1.1 Clinical manifestation, transmission, and pathogenesis of EV-A71 infection	3
2.1.2 Virology and genome organization of EV-A71	7
2.1.2.1 Structural proteins	8
2.1.2.2 Non-structural proteins	9
2.1.3 Steps of replication cycle of EV-A71	12
2.2 Drug repurposing for EV-A71	14
2.2.1 Direct-acting repurposed antiviral (DARA)	15
2.2.2 Host-targeting repurposed antiviral (HTRA)	16

TABLE OF CONTENTS (Cont.)

	page
CHAPTER 3 OBJECTIVE	20
3.1 Ultimate objective	20
3.2 Specific objectives	20
CHAPTER 4 RESEARCH METHODOLOGY	
4.1 Experimental outline	21
4.2 Virus propagation	22
4.3 Evaluation of cytotoxicity of 153 antiviral compounds of the MMV Pandemic Response Box to rhabdomyosarcoma (RD) cells by sulforhodamine B (SRB) assay	23
4.3.1 Preparation of working antiviral compounds	23
4.3.2. Cytotoxicity assay	23
4.4 Screening of compounds with potential anti-EV-A71 activity	24
4.5 Dissecting mechanism of the inhibitory effect of the hit compounds on EV-A71 replication	25
4.5.1 Sample preparation	25
4.5.2 qRT-PCR	26
4.5.3 Western bolt analysis	28
4.5.4 CCID ₅₀ assay	29
4.5 Statistic analysis	30

TABLE OF CONTENTS (Cont.)

	page
CHAPTER 5 RESULTS AND DISCUSSION	31
5.1 Virus propagation	32
5.2. Evaluation of Cytotoxicity of Antiviral Compounds of the MMV Pandemic Response Box	33
5.3 Screening of Compounds with Potential Anti-EV-A71 Activity	34
5.4 Dissecting Mechanism of Inhibitory Effect of the Hit Compounds on EV- A71 Replication	39
CHAPTER 6 CONCLUSIONS AND RECOMMENDATIONS	44
CHAPTER 7 CONCLUSIONS AND RECOMMENDATIONS	51
REFERENCES	52
APPENDICES	
APPENDIX A	64
APPENDIX B	65
APPENDIX C	66
APPENDIX D	68
BIOGRAPHY	69

LIST OF TABLES

Tables	Page
2.1 Selected EV-A71 antivirals with translational potential	16
5.1 Chemical structures, alternative names, and mode of action of the selected hit compounds.	36



LIST OF FIGURES

Figures	Page
2.1 Photograph shows manifestation of hand-foot-mouth disease	3
2.2 Schematic drawing manifestation of hand-foot-mouth disease	6
2.3 Diagram depicts genome organization and antigenic determinants of EV-A71	7
2.4 Schematic drawing diagram depicts replication cycle of EV-A71	13
2.5 (A) Schematic diagram of enterovirus type I IRES bound by human eIF4G1, PABP, eIF4E, eIF4A, and eIF3 and ribosome. (B) Structural domains of the IRES and regions	13
5.1 Determination of EV-A71 viral titer by cell culture infectious dose 50 (CCID ₅₀)	31
5.2 Cytotoxicity of Antiviral Compounds of the MMV Pandemic Response Box	33
5.3 Compounds with Potential Anti-EV-A71 Activity	35
5.4 A representative standard curve of VP1 used to calculate EV-A71 RNA number copies	40
5.5 Anti-EV-A71 activity by virus reduction assays for viral RNA copy numbers using qRT-PCR.	41
5.6 Anti-EV-A71 activity by virus reduction assays for viral protein synthesis using Western blot analysis and densitometry	42
5.7 Anti-EV-A71 activity by virus reduction assays for the release EV-A71 virions using CCID ₅₀ assay.	43
6.1 Superimposition of EV-A71 3C and HRV 3C–AG7088 structures.	45
6.2 Schematic diagram of the crystal structure of HRV 3C complexed with the 2-pyridone-containing peptidomimetics	47
6.3 Structure-based multiple-sequence alignment of 3C proteases of different picornaviruses	48

LIST OF ABBREVIATIONS

Symbols/Abbreviations	Terms
+ssRNA	Positive-sense, single-stranded RNA
2Apro	2A protease
3CDpro	3CD protease
3Cpro	3C protease
3Dpol	3D polymerase
ACBD3	Acyl-coenzyme A-binding domain-containing 3
ATP1B3	$\beta 3$ subunit of Na ⁺ /K ⁺ -ATPase
BBB	Blood-brain barrier
CV-A6	Coxsackievirus A6
cDNA	Complementary deoxyribonucleic acid
CT	Cycle threshold
Ca ²⁺	Calcium ion
CNS	Central nervous system
DARA	Direct-acting repurposed antiviral
EV-A71	Enterovirus 71
ER	Endoplasmic reticulum
eIF4G1	Eukaryotic translation initiation factor 4-gamma 1
eIFs	IRES-specific cellular trans-acting factors
FDA	Food and Drug Administration
HFMD	Hand, foot, and mouth disease
HTRA	host-targeting repurposed antiviral
IL	Interleukin

LIST OF ABBREVIATIONS (Cont.)

Symbols/Abbreviations	Terms
IFN γ	Interferon-gamma
IRES	Internal ribosomal entry site
ITAFs	IRES trans-acting factors
IRF7	IFN regulatory factor 7
NPC	Nuclear pore complex
ORF	Open reading frame
PE	Pulmonary edema
PSGL-1	P-selectin glycoprotein ligand-1
RD cells	Rhabdomyosarcoma cells.
RO	Replication organelle
RdRp	RNA-dependent RNA polymerase
SCARB2	Scavenger receptor class B member 2
SRB assay	Sulforhodamine B assay
SH-SY5Y cells	Human Neuroblastoma Cell Line (ATCC CRL-2266)
TM	Transmembrane domains
TNF α	Tumor necrosis factor-alpha
TRIF	TIR-domain-containing adapter- inducing interferon- β
UMP	Uridine monophosphate
VP	Virion proteins
VPg	Virus genome-linked protein

CHAPTER 1

INTRODUCTION

Hand, foot, and mouth disease (HFMD) is a viral infection caused by enteroviruses including enterovirus 71 (EV-A71), coxsackievirus A6 (CV-A6), CV-A10, and CV-A16 commonly found in children under the age of 5 years.¹ Clinical manifestations of HFMD range from asymptomatic, flu-like symptoms to vesicular rashes scattered on palms, feet, buttocks, and oral mucosae which are self-limited to fatal neurological complications. The neurological complications of HFMD are usually associated with EV-A71 infection including meningitis, encephalitis, acute flaccid myelitis (AFM), and neurogenic cardiopulmonary failure.¹⁻² HFMD outbreaks have been found worldwide but the high disease burden has been confined to Asia-Pacific countries as it has established endemicity in the area for decades.¹⁻² The viruses that cause HFMD are responsible for millions of infections in East and Southeast Asia per annum.¹ It has been estimated that 6% of the symptomatic cases are hospitalized. Among the hospitalized cases, 18.7% of them are expected to develop complications and 5% of such cases are fatal.¹ Currently, vaccines for preventing HFMD are limited to use only in China. Moreover, antiviral drugs effective against EV-A71 have not been found in clinical practice to mitigate neurological complications. Therefore, there is a need to develop vaccines and specific antiviral drugs against the EV-A71 infection.

Even though vaccines are recognized as a preferred promising line of defense against virus outbreaks, vaccine development is a complex process, and multiple challenges are involved in unknown biology and high genetic variability of the pathogen. Hence, this leads to the contemporary unavailability or reduced efficacy of vaccines. Therefore, antiviral drugs are more promising for combating those viruses meanwhile an effective vaccine is unavailable. Nowadays, the drug discovery for emerging or re-emerging viruses has been accelerated by exploring new molecular pathways and targets for intervention of the well-characterized drugs, either approved or under investigation, to identify new treatment of virus infections that beyond the original indicative scope, namely “drug repurposing”.³ Given the repurposed drugs have been proven to be safe in humans, they can reduce not only the attrition rate to be

a novel antiviral but also time and resource-consuming for drug development. Drugs with repurposing potential against viral diseases have been identified mostly by screening small-molecule libraries containing approved and investigational drugs, and natural compounds.⁴ These libraries are available as open-source or commercial.⁵ Hence, in this thesis, it could be expected that antiviral drugs against EV-A71 can be repurposed from the open-source drug library.

In 2019, an open-source drug library namely MMV Pandemic Response Box was launched by the Medicines for Malaria Venture (MMV) in collaboration with the Drugs for Neglected Diseases initiative (DNDi) to accelerate drug discovery efforts against the emerging pandemic. The MMV Pandemic Response Box is a chemically and pharmacologically diverse mixture of early-stage, emerging anti-infective scaffolds, and more mature compounds currently undergoing clinical development that combines 201 antibacterial, 46 antifungal, and 153 antiviral agents in the 96-well plate format. It was hypothesized that the antiviral agents included in the Pandemic Response Box might bind and interfere with target molecules or cellular pathways that are conserved or shared among the closely related viruses with the EV-A71.

In this thesis proposal, we proposed to screen 153 antiviral agents of the Pandemic Response Box for repurposing against EV-A71 infection and investigate the inhibitory effects on viral replication. The benefit of this study will provide a new treatment regimen and open the therapeutic avenue to counteract EV-A71 infection, Thailand's major public health problem.

CHAPTER 2

REVIEW OF LITERATURE

2.1 Enterovirus A71 (EV-A71)

2.1.1 Clinical manifestation, translation, transmission, and pathogenesis of EV- A71 infection

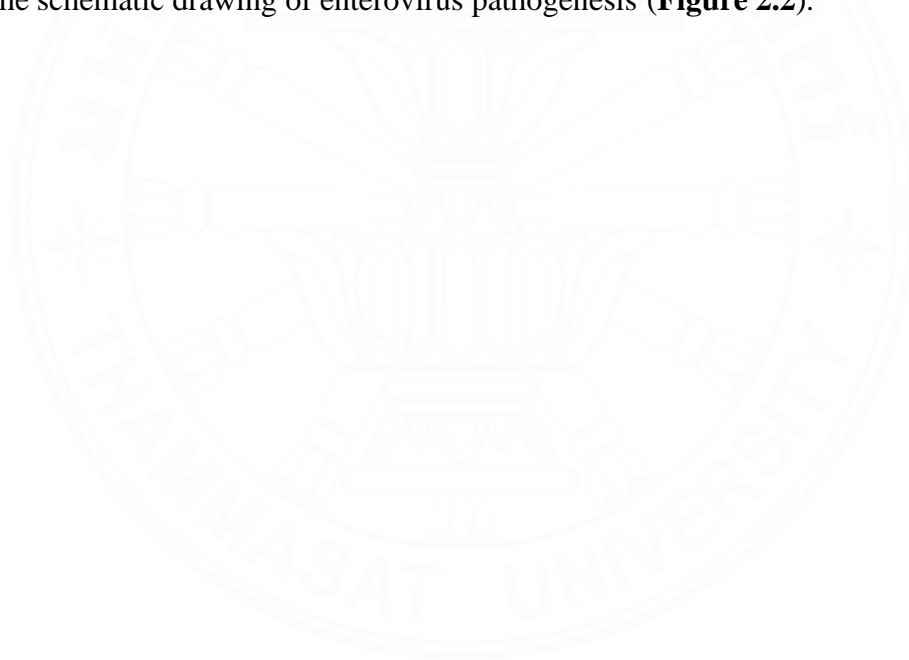
EV-A71 infection can manifest hand-foot-mouth disease (HFMD) associated with neurological complications that are mostly found in children at age below 5 years old. The disease is transmitted person-to-person through the fecal-oral route or ingesting infectious secretions such as mucous and saliva. The incubation period for HFMD ranges from 3 to 7 days before the appearance of symptoms and peaks within one week of disease onset. Clinical manifestations of EV-A71 infection range from asymptomatic to involvement of the upper respiratory tract, gastrointestinal tract, central nervous system, and cardiovascular system.⁶⁻⁸ Up to 71% of EV-A71 infections in children may be asymptomatic which serve as a reservoir for transmission. Most cases manifest mild symptoms which is self-limiting. Mild clinical symptoms could range from high fever, vomiting, vesicular rashes on palms and feet, ulcers in the oral cavity, loss of appetite, and diarrhea as represented in Figure 2.1.^{1,6-8} EV-A71 can invade the central nervous system (CNS) and result in fatal neurological complications including meningitis, encephalitis, and neurogenic cardiopulmonary failure which is the major cause of death.^{1,6,9}



Figure 2.1 Photograph shows manifestation of hand-foot-mouth disease including vesicular rashes on palms and the tongue. ¹

After viruses get into the human body by ingestion, the ingested viruses infect cells of the oropharyngeal mucosa and regional lymphoid tissue such as tonsillar crypts where they establish primary replication, then spread and perform secondary replication in Peyer's patches of gastrointestinal tract. These tissues support the replication of EV-A71 by expressing cellular receptors for the virus attachment and entry including PSGL1 and SCARB2.¹⁰ At this phase, the infection is normally terminated by host innate immunity resulting in asymptomatic manifestation. If the viruses further disseminate into various organs including lungs, heart, liver, pancreas, mucosal membranes, skin, or even central nervous system (CNS) through blood circulation, the infection causes viremia.^{1,9,11} In viremic phase, the viruses disseminate not only to those organs but also to the intestines for shedding with feces and transmitted by person-to-person. The viremia triggers inflammatory responses resulting in systemic and local symptoms such as fever and tissue injury and skin lesions, respectively. Subsequently, the infection activates adaptive immune responses to mount effective anti-virus immunity leading to virus clearance and disease resolution. In severe HFMD, EV-A71 can invade and infect the CNS as it has been identified as a neurotropic virus resulting in neurological complications. Nevertheless, the mechanism of neuropathogenesis by EV-A71 infection has not been elucidated yet. It is postulated that viruses may get into the CNS by two hypothetical mechanisms including retrograde axonal transport and hematogenous transmission through blood-brain barrier (BBB).¹¹⁻¹² For retrograde axonal transport, the EV-A71 may get entry into axons of the peripheral nerve and is transported retrogradely to the cell body of neurons in the CNS. For the hematogenous transmission model, the infected leukocytes carrying EV-A71 acts as Trojan horse traffic through blood circulation and arrive at the inflamed BBB which has lost the integrity allows the infected leukocytes adhere and extravasate (diapedesis) into brain parenchyma. However, the detailed mechanisms of the two models have not been elucidated yet. The infiltration of the CNS by infected leukocytes or infection by the viruses cause massive local inflammation leading to inflammation and tissue injury of meninges, brain parenchyma, and brainstem as well as aberrant death of neurons and astrocytes.¹³ Furthermore, it was known that acute cardiopulmonary edema (PE) with or without hemorrhage is subsequences of the severe

CNS infection by EV-A71, but the mechanism is not elucidated yet. It has been reported that overproduction of proinflammatory cytokines; called a cytokine storm, such as interleukin (IL)-1 β , IL-6, IL-10, IL-12, IL-13, tumor necrosis factor-alpha (TNF α), and interferon-gamma (IFN γ), is associated with systemic inflammatory responses leading to acute cardiopulmonary edema.¹¹⁻¹³ It has been postulated that the systemic inflammation may lead to increase of blood sympathetic pressure by that it increases capillary hydrostatic and permeability of pulmonary blood vessel.¹²⁻¹³ Moreover, inflammation of the CNS causes massive release of catecholamines into blood circulation leading to cardiac damage and increased pulmonary vascular permeability and leakage. Taken together, it has been suggested that development of cardiopulmonary failure caused by the EV-A71 infection is neurogenic cause as shown in the schematic drawing of enterovirus pathogenesis (**Figure 2.2**).¹⁴⁻¹⁵



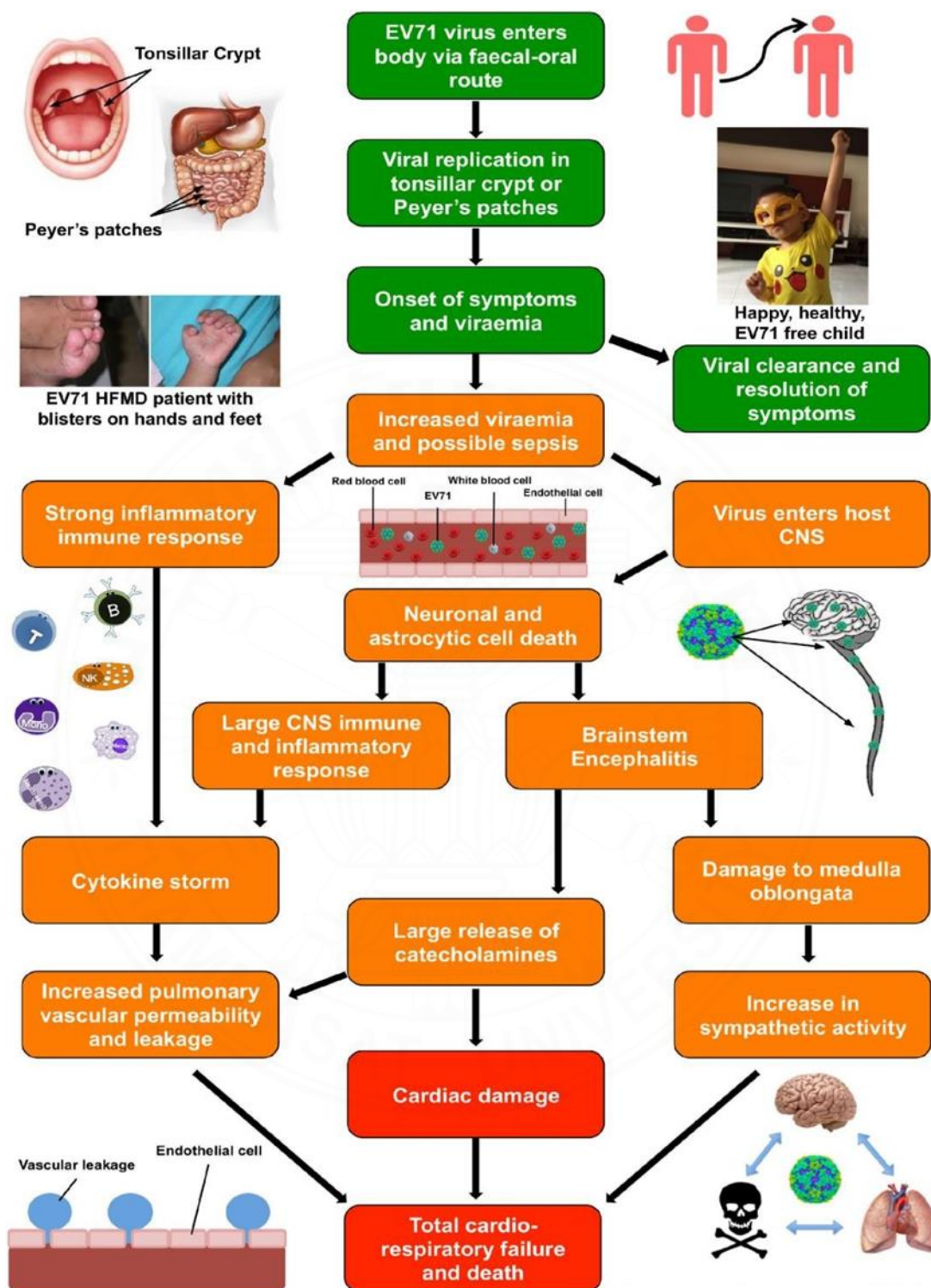


Figure 2.2 Schematic drawing of enterovirus pathogenesis. ³³

2.1.2 Virology and genome organization of EV-A71

Enterovirus A71 (EV-A71) is an RNA virus belonging to the family *Picornaviridae*, genus *Enterovirus*, species *Enterovirus A*. The EV-A71 particle is a non-enveloped, icosahedral capsid that encloses a positive-sense, single-stranded genomic RNA. The EV-A71 genome is approximately 7.4 kb in length and contains a single open reading frame (ORF) flanked by untranslated region at 5'- and 3'- termini designated as 5'- and 3'- UTR, respectively. 5'-UTR contains structure complexity of mRNA called internal ribosomal entry site (IRES) for mediating cap-independent translation of viral genome. While 3'-UTR is polyadenylated. The ORF of the EV-A71 genome is subdivided into three sub-regions of protein-coding sequences namely P1, P2, and P3 which are initially translated into a single polypeptide and then cleaved by proteases to yield individual mature proteins later. The P1 region encodes four structural virion proteins (VP) including VP1, VP2, VP3, and VP4. The P2 and P3 regions encode seven non-structural proteins including 2A, 2B, and 2C generated from the P2 and 3A, 3B, 3C, and 3D from the P3 which play important roles in viral replication and manipulation and interference of cellular activities and evasion of anti-virus immunity in host cells as represent in **Figure 2.3**.¹⁶

Herein, the functions of each EV-A71 protein and the steps of viral replication will be mentioned to point out their potential for being drug targets.

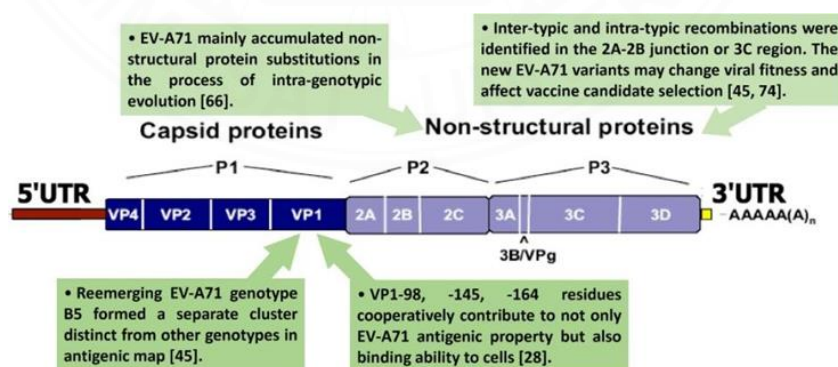


Figure 2.3 Diagram depicts genome organization and antigenic determinants of EV-A71.¹⁶

2.1.2.1 Structural proteins

The icosahedral capsid of EV-A71 is 22-30 nm in size and composed of 60 identical protomers containing four VP1 to VP4. This viral capsid encloses single-stranded positive-sense RNA. VP proteins form an eight-stranded anti-parallel β -barrel structure in the form of a wedge that facilitates packing looks like β -sandwich “jelly-roll” folds.^{16,18} Each of VP is assembled to form 2-, 3- and 5-fold rotational symmetry axes capsid. The VP1 to VP3 are exposed on the outer surface of the virion, while VP4 is beneath the capsid shell. There is a depression region called the canyon located around each icosahedral 5-fold axis on the surface of the viral capsid which facilitates cellular receptor binding.¹⁶

1) VP1 is composed of 297 amino acids. On the virion, VP1 on each protomer constitutes a canyon. The region beneath the canyon is a hydrophobic pocket containing a lipid molecule known as “pocket factor” that functions to stabilize the virion. After EV-A71 infects the host cell and gets entry into the cytoplasm by receptor-mediated endocytosis, VP1 binds with PSGL-1 and SCARB2 receptors and mediates dislodging of the pocket factor leading to conformational change of the capsid to undergo a two-step uncoating process. First, the capsid is expanded by the formation of gaps along the 2-fold axes leading to exposure of the N-termini of VP1 and VP4 to the external part of the capsid and change in density and antigenicity of the particle called altered particle or A-particle.¹⁸⁻¹⁹ Then, the N-termini of VP1 are inserted into an endolysosomal membrane to immobilize EV-A71 particles on the membrane. In contrast, the N-termini of VP4 protein forms a pore on the endolysosomal membrane by oligomerization to pass through the genomic RNA across the endosomal membrane into the cytosol. These processes contribute to the pathogenesis of EV-A71 infection. In addition, VP1 has been reported to activate endoplasmic reticulum (ER) stress and promote the upregulation of cell surface-exposed calreticulin that important mediator for phagocytosis of viable neurons by the microglia.¹⁹

2) VP2 consists of 254 amino acids. It has several neutralization linear epitopes which are shared among the strains of EV-A71 especially the residues 136–150.^{16-17,21} A mutant virus with lysine to methionine substitution at

residuals XX or glutamine to glutamic acid substitution at residuals XX on the VP2 showed increasing of viral titers and enhancing apoptosis in the infected cells.²⁰ Moreover, the synergistic effect of VP2 double mutations enhanced viral binding and contributing to viral infectivity in vitro.

3) VP3 consists of 245 amino acids. It has been reported that the amino acid residues 59–67 of VP3 are more highly conserved between the subgenogroups. Moreover, conformational epitope on the knob of EV-A71 VP3 encompasses residues 55 to 69 has been reported.^{17,21}

4) VP4 consists of 69 amino acids which is myristoylated to confer stability to the capsid. The VP4 has an extended conformation and is present inside the virion. It is conferring stability to the capsid.^{17,22} Because VP4 is more conserved among EV-A71 strains than VP1, VP2, and VP3, hence, it has been intensively studied for vaccine development.

2.1.2.2 Non-structural proteins

1) EV-A71 2A proteinase (2A^{pro}) is a cysteine proteinase that contains approximately 150 amino acids. It has been demonstrated to play a role in replication and pathogenesis.^{17,23} The crystal structure of 2A^{pro} demonstrates a chymotrypsin-like fold. The active site is composed of the catalytic triads made of C110A, H21, and D39. The N-terminal domain has a loop and hydrophilic surface for host protein recognition. While the C-terminal domain is folded to form the structure of a double β -turn hydrophobic motif and acidic motif whose functions are essential for viral replication.²³ The protease activity of 2A^{pro} is associated with viral pathogenesis, apoptosis induction, and immune evasion of host cells.²³⁻²⁴ The positive regulation of viral replication by the ERK cascade was reported by associating both *cis*-cleavage of the viral polyprotein and *trans*-cleavage of the cellular eIF4GI by the 2A^{pro}.²⁵ The 2A^{pro} is responsible for *cis*-cleavage of the enteroviral nascent polyprotein at the peptide bond between VP1 (C-terminal) and P2 (N-terminal of 2A protein) and cleave 3CD intermediate product to yield mature 3C and 3D.^{20,23-24} The 2A^{pro} mediates *trans*-cleavage of eukaryotic translation initiation factor 4-gamma 1 (eIF4G1) of the host to shut-down cellular translation which gears the factors to translate the viral genome

instead. The suppression of cellular translation can induce apoptosis. Moreover, 2A^{pro} cleaves type I interferon receptor; IFN- α/β receptor 1, to block IFN-induced Jak/STAT signaling pathway attributes to the evasion of innate anti-viral immunity.²³⁻²⁴

2) EV-A71 2B protein is an ion channel protein belonging to viroporin family. A monomeric 2B contains approximately 97 to 99 amino acids with two transmembrane domains (TM1 and TM2).^{16-71,25} Enteroviral 2B proteins have been demonstrated to localize on plasma membranes and organelles such as mitochondria, ER, and Golgi. 2B protein of EV-A71 was found to be inhibited by an antagonist of chloride ion channel which indirectly affected the increase of intracellular Ca²⁺.²⁵ Inhibition of chloride conductance activity of the EV-A71 2B by pleconaril was reported to suppress virus release.³² Supasorn O., et al (2019) reported that EV-A71 2B protein induced a caspase-dependent apoptotic cell death and elevation of cytosol Ca²⁺ which likely associated with ER-mitochondrial pathway in human neuronal SH-SY5Y cells.⁽²⁵⁾ Interaction between EV-A71 2B and proapoptotic protein Bax leading to redistribution of the Bax to mitochondria has been reported to induce cell apoptosis by mitochondrial pathway.²⁵⁻²⁶

3) EV-A71 2C protein contains 329 amino acids and mainly functions as an NTPase. The amino acids located at residues 5–43 on the N-terminus of 2C potentially have membrane-binding activity. It is involved in the rearrangement of the host cell membrane formed into replication organelle (RO) to support virus replication. The 2C links double-stranded viral RNA to the RO by associating with the ER protein 3 of host cells. Moreover, enteroviral 2C can reduce the formation of the predominant form of NF- κ B (heterodimer p65/p50) by interacting with the IPT domain of RelA(p65) and blocking NF- κ B activation leading to antagonizing innate anti-virus immunity.^{16,27}

4) EV-A71 3A protein is a membrane-bound protein containing 86 amino acids. The N-terminus of 3A is proline rich region and is involved in protein–protein interactions with host factors. EV-A71 3A protein interacts with a host factor acyl-coenzyme A-binding domain-containing 3 (ACBD3) leading to recruitment of PI4KB to form a large complex of RO that is essential for RNA synthesis.^{16,28} Interaction of EV-A71 3A with human β 3 subunit of Na⁺/K⁺-ATPase

(ATP1B3)protein has been reported to enhance the production of type-I IFN resulting in inhibition of EV-A71 replication.¹⁶⁻¹⁷

5) EV-A71 3B protein, also alternatively called virus genome-linked protein (VPg), is a nucleic acid chaperone protein and composed of approximately 22 amino acids. It is essential for picornavirus RNA replication by uridylylation. The crystal structure of the EV-A71 3Dpol-VPg complex showed that VPg was anchored at the bottom of the palm domain of the 3Dpol molecule.¹⁶⁻¹⁷ The VPg uridylylation reaction involves the binding of VPg to 3Dpol to transfer of uridine monophosphate (UMP) by 3Dpol to the hydroxyl group of the third amino acid Tyr of VPg.¹⁶

6) EV-A71 3C protease (3Cpro) is a cysteine protease containing 184 amino acids. Enteroviral 3Cpro has a typical chymotrypsin-like fold which is similar to 2Apro. At the base of the surface loop denoted as β -ribbon, Gly123 and His133 form hinges which are important for the proteolytic activity of EV-A71 3Cpro. During viral genome translation, 3Cpro cleaves itself from the P3 precursor protein to be active mature protein which turn to cut P2 and P3 to generate the remaining mature proteins. Besides proteolytic activity, EV-A71 3Cpro has been reported to elicit RNA-binding activity.¹⁶⁻¹⁷ Recently, 3Cpro has been found to contain a virulence determinant involved in EV-A71 infection which is located on the 69th residue.²⁸ EV-A71 3Cpro plays a critical role in immune evasion by cleaving the adaptor protein TRIF (TIR-domain-containing adapter-inducing interferon- β) and IFN regulatory factor 7 (IRF7) to dampen immune responses.^{16-17,28}

7) EV-A71 3D polymerase (3D^{pol}) contains approximately 462 amino acids and possesses an Mn²⁺-dependent, RNA-dependent RNA polymerase(RdRp) responsible for viral RNA replication.¹⁶ The enteroviral 3D^{pol} has six conserved motifs namely A, B, C, D, E, and F in which each of them containing four- amino-acid-long sequences. It has been reported that the 3D^{pol} could modulate the expression of S-phase control proteins that play a role in cell arrest in the S phase. Moreover, EV-A71 3D^{pol} can stimulate the activation of NLRP3 inflammasome and the release of IL-1 β through direct binding to NLRP3 leading to the assembly of inflammasome complex by forming a 3D^{pol}-NLRP3-ASC (the apoptosis-associated

speck-like protein possessing a caspase-recruiting domain) ring-like structure resulting in the activation of IL-1 β .²⁷ The role in immune evasion of 3D^{pol} has been reported to attenuate IFN- γ signaling accompanied by a decrease in STAT1 expression.^{16,27}

2.1.3 Steps of replication cycle of EV-A71

The viral replication cycle is a multistep process composed of viral entry, genome uncoating, genome translation and replication, particle assembly (morphogenesis), and egression. After the EV-A71 gets into the host cell, its genome is directly translated and processed into viral proteins which subsequently take control of cellular metabolism and biosynthesis processes and subvert host immune responses that favor establishing a productive viral infection.¹⁷

The EV-A71 replication cycle is generally like the closely related enteroviruses in which poliovirus (PV) is a prototype. EV-A71 initially recognizes and attaches to host cellular receptors on the cell surface (**Figure 2.4**). The main cellular receptors of EV-A71 are human scavenger receptor class B member 2 (SCARB2) and human P-selectin glycoprotein ligand-1 (PSGL-1).¹⁶⁻¹⁷ The binding of the receptor triggers endocytosis of the EV-A71 particles attaching to the cell membrane. The binding of capsid canyon to receptor facilitates destabilization of the viral particle leading to the uncoating of the virus genome released into the cytoplasm. The released RNA genome serves as the mRNA template for IRES-mediated translation of the polyprotein which is processed by the viral protease 2A^{pro} and 3C^{pro} into precursors and mature proteins. The IRES-mediated translation requires the binding of IRES-specific cellular *trans*-acting factors (ITAFs) and canonical eukaryotic initiation factors (eIFs).²⁹ Normally, almost of ITAFs are nuclear-resident molecules that shuttle between the nucleus and cytoplasm compartment in the control of the nuclear pore complex (NPC) as shown in **Figure 2.5**.²⁹

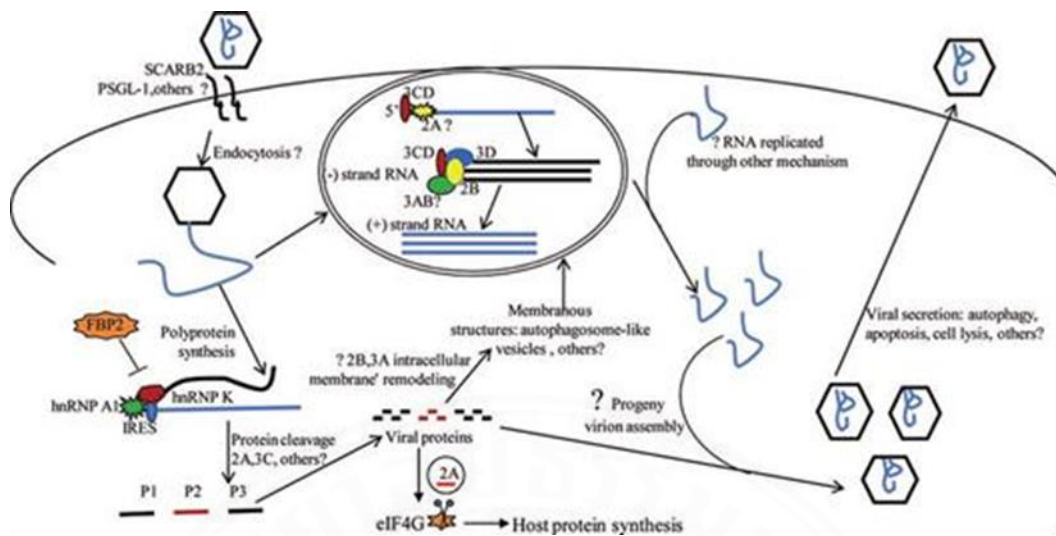


Figure 2.4 Schematic drawing diagram depicts replication cycle of EV-A71.⁽³⁵⁾

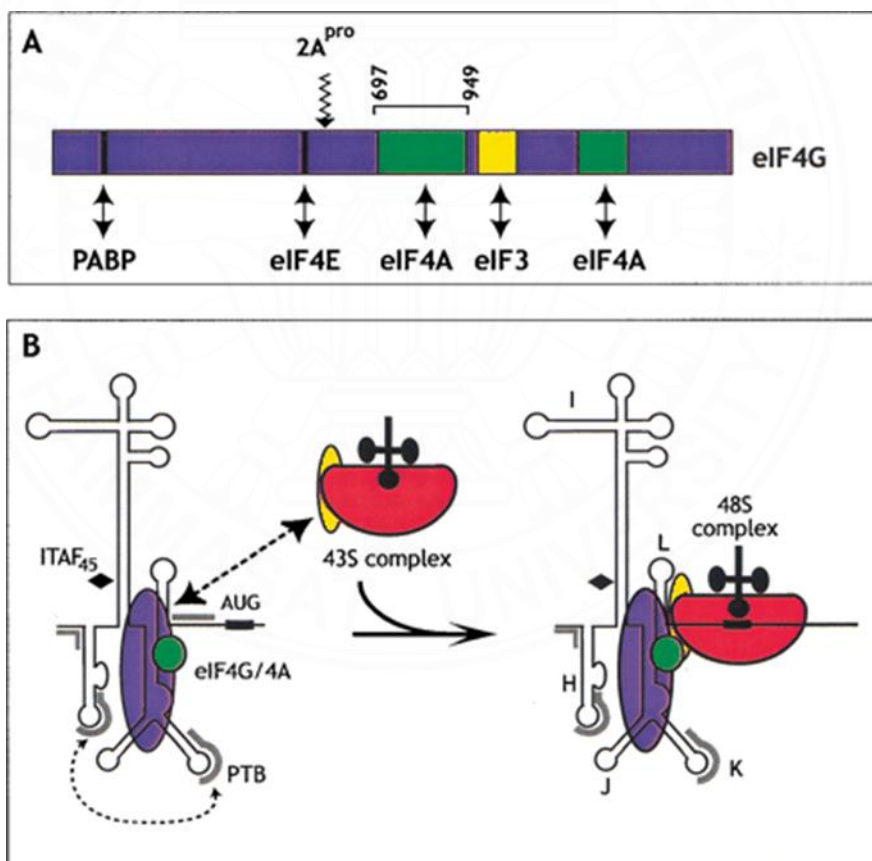


Figure 2.5 (A) Schematic diagram of enterovirus type I IRES bound by human eIF4G1, PABP, eIF4E, eIF4A, and eIF3 and ribosome. (B) Structural domains of the IRES and regions of contact with the following factors shown eIF4G/4A complex (blue/green), ITAF 45 (diamonds), PTB (gray).³³

The basal level of ITAFs in the cytoplasm may limit the efficiency of EV-A71 genome translation and replication. Therefore, EV-A71 employs viral 2A^{pro} and 3C^{pro} to disrupt NPC leading to the accumulation of ITAFs in the cytoplasm of the infected cells. Moreover, several eIFs and ITAFs are cleaved by enteroviral proteases resulting in host transcription and translation shut-off and deviating from these factors to enhance viral genome translation.^{17,29} The mature nonstructural proteins including 3D^{pol}, 3AB, VPg, and 2C remodel the organelle membranes to form the RO to serve as a scaffold facilitating genomic RNA replication. At the viral RO, the genomic RNA serves as a template for the synthesis of complementary negative-sense RNA which then turns to be a template for synthesis of a newly synthesized genomic positive-sense RNA. The double-stranded RNA intermediate is unwound by viral 2C^{Hel}. Lastly, at the viral replication complex, the newly synthesized +ssRNA genome is encapsidated into virus capsid to produce the mature virus particle. Then, the new progenies or the mature virions are released from the infected host cells by cell lysis or a not yet clearly understood mechanism.¹⁷

2.2 Drug repurposing for EV-A71

Most of the emerging and re-emerging viral diseases such as Ebola, MERS, SARS, SARS-CoV-2, and EV-A71 lack specific antiviral drugs.³⁰ This is due to limited knowledge of pathogenesis. Moreover, the traditional drug development approach commonly takes approximately 10 years from pre- and clinical trial phases to license the approved drug for market availability.³⁰ Nevertheless, only 5% of drug candidates in the clinical trial phase are finally approved.³⁰ Hence, traditional drug development is time- and resource-consuming. To overcome these drawbacks, drug repurposing has become an alternative approach for drug discovery to treat viral infections. Drug repurposing is a strategy for identifying either a new target or indication as well as the same target of new virus of the approved or investigational drugs that are beyond the original scope or indication.^{3,30} By using drugs that are known for their safety profile, the phase I clinical trial could be skipped leading to a reduction of attribution rate to be

an approved antiviral drug. Hence, drug repurposing could significantly accelerate antiviral development for emergency use.

Typical steps of drug repurposing comprise identification of drug candidates, efficiency confirmation and mechanistic analysis in animal models, antiviral efficiency analysis in clinical trials, and approval of the novel indication by governmental agencies.^{3-4,30}

Identification of repurposed drug candidates for the novel indication or target could be performed by *in silico* or *in vitro* screening. For *in silico* screening, the method relies on computational analysis of the interaction between target and drug molecule. Hence, the data on the structure of the interacting molecules must be known or predictable. For *in vitro* screening, the method involves high throughput antiviral screening mainly in cell culture-based model leading to validation for the most potent candidates.

The repurposed antiviral agents are categorized based on their inhibitory mechanism into two groups including direct-acting repurposed antiviral (DARA) and host-targeting repurposed antiviral (HTRA).^{3,30}

2.2.1 Direct-acting repurposed antiviral (DARA)

Since viruses are obligate intracellular parasites, their replication depends solely on cellular factors and must take place within the living host cells. The infecting virus must take control of cellular activities to favor its benefit using virally encoded proteins or complex structures of the genome. Therefore, antiviral drugs directly target the viral proteins or factors, namely DARA, which could inhibit virus replication. DARAs activity relies on structure similarity or identity of viral proteins that are shared among the related viruses, particularly RdRp, proteases, helicase, ion conductance proteins, and capsid.^{4,30}

The DARAs of EV-A71 have been reported including inhibitors of capsid, 3A, 2C^{pro}, 3C^{pro}, 3D^{pol}, and IRES (**Table 2.1**).³¹ DARAs that have inhibitory activity against viral enzymes could interfere with the respective steps in the replication cycle. Capsid inhibitors prevent conformational changes of the capsid leading to

inhibition of genome uncoating. While IRES inhibitors block ITAFs or canonical translational factors binding resulting in suppression of viral genome translation.

2.2.2 Host-targeting repurposed antiviral (HTRA)

Cellular proteins or pathways that are required and indispensable for virus replication cycle including viral entry, genome uncoating, genome translation and replication, virion assembly, and egress are targets of HTRAs. Advantages of HTRAs include broad-spectrum antiviral activity and a high genetic barrier to drug resistance.³¹ However, most of the antiviral drug discovery has been focused on viral targets and most of the approved antiviral drugs are DARAs.³⁰ Most importantly, the cytotoxicity offers a potential issue with host-targeting antivirals. For instance, chloroquine, an antimalarial drug, was found to inhibit EV-A71 replication in cell culture.³¹ Even though the mechanism has not been exactly elucidated, the lysosomotropic property of chloroquine which could inhibit lysosome functions might be attributable to the uptake impairment of the virus.³¹ Related papers reported the PI4KB-PI4P-OSBP pathway was exploited by enteroviruses to direct cholesterol to the replication organelles. The inhibitors against the PI4KB-PI4P-OSBP pathway have been reported as being EV-A71 HTRA (Table 2.1).³¹

Table 2.1 Selected EV-A71 antivirals with translational potential.³²

Inhibitor	Remark	Inhibited	Not inhibited
Capsid inhibitors			
Pleconaril	Activity against EV-A71 is controversial Dropped out of clinical trial for rhinovirus infection	EV-D68, RV-87, RV-A, and RV-B	PV-1, RV-B17, RV-A45, RV-C
Vapendavir	Dropped out of clinical trial for rhinovirus infection	EV-A71, EV-C, RV-A, and RV-B	EV-D68
Pirodavir	Dropped out of clinical trial for rhinovirus infection	EV-A71, EV-D68, EV-A, EV-B, EV-C, EV-D, RV-A, and RV-B	RV-A8, RV-A25, RV-A45, RV-87, and RV-C

Table 2.1 Selected EV-A71 antivirals with translational potential (Cont.).³²

Inhibitor	Remark	Inhibited	Not inhibited
PR66	<i>In vivo</i> antiviral efficacy against EV-A71 in mice	EV-A71	EV-D68, CV-A16, CV-B1, CV-B2, CV-B3, Echovirus 9, rhinovirus
Capsid inhibitors			
NLD-22	Favorable PK properties <i>In vivo</i> antiviral efficacy against EV-A71 in mice	EV-A71	—
VP1-14	Favorable PK properties <i>In vivo</i> antiviral efficacy against EV-A71 in mice	EV-A71	—
ICA135	<i>In vivo</i> antiviral efficacy against CV-A10 in mice	CV-A10, EV-A71, CV-A16, CV-B3, PV-1, EV-D68	—
CB-30	Binds to the five-fold axis of the EV-A71 capsid	EV-A71, HIV-1, HIV-2	—
Suramin	Polypharmacology <i>In vivo</i> antiviral efficacy against EV-A71 in mice and rhesus monkeys	EV-A71, CV-A2, CV-A3, CV-A10, CV-A12, CV-A16, CV-A9, ECHO25	ECHO20, PV1-3, EV-D68
Brilliant black BN (E151)	Binds to the five-fold axis of the EV-A71 capsid <i>In vivo</i> antiviral efficacy against EV-A71 in mice	EV-A71, CV-A16, CV-A6	CV-A4, CV-A10
2C inhibitor			
(S)-Fluoxetine	Lack of efficacy against EV-D68 in clinical trials (S)-Enantiomer is more active	CV-B3, EV-D68, HRV-A2, and HRV-B14	EV-A71, PV-1
2C-12b	Analog of fluoxetine	EV-A71, EV-D68, CV-B3, PV-1, CV-	—

Table 2.1 Selected EV-A71 antivirals with translational potential (cont.).³²

Inhibitor	Remark	Inhibited	Not inhibited
3Dpol inhibitor			
Gemcitabine	Identified through drug repurposing; Synergistic effect with interferon- β	EV-A71, EV-D68, CV-B3, CV-A6, CV-A16, E-7, PV-1, DENV, and CHIKV	—
3Dpol inhibitor			
Sofosbuvir	<i>In vivo</i> antiviral efficacy against EV-A71 in mice	EV-A71	—
FNC	HIV clinical candidate	EV-A71, CV-A16, CV-A6, EV-D68, and CV-B3	—
Favipiravir (T-705)	Synergistic effect with suramin	EV-A71, EV-D68 (not all subtypes)	—
NITD008	Failed in clinical trial for flavivirus infection	EV-A71	—
IRES inhibitor			
DMA-135	Binds to the IRES stem loop 2	EV-A71	—
Prunin	Mutations in IRES confer drug resistance; <i>In vivo</i> antiviral efficacy against EV-A71 infection in mice	EV-A71	—
Emetine	<i>In vivo</i> antiviral efficacy against EV-A71 infection in mice	EV-A71, CV-A16, CV-B1, EV-D68, Echovirus 6	—

Table 2.1 Selected EV-A71 antivirals with translational potential (Cont.).³²

Mechanism	Inhibited	Not inhibited
Host-targeting antivirals		
Decreases OSBP level	EV-A71, CV-B3, CV-A21, and RV-B14	—
Allosteric inhibitor of PI4KB	RV-1, RV-2, RV-8, RV-64, PV-2, EV-A71, EV-D68	—
DHODH inhibitor	HCV, DENV, ZIKV, CHIV, EV-A71, HIV, RSV	—

CHAPTER 3

RESEARCH OBJECTIVE

The main objective of this study is to screen 153 antiviral agents of the Pandemic Response Box that have an inhibitory effect on EV-A71 infection in rhabdomyosarcoma (RD) cells.

3.1 Specific objectives

3.1.2 To screen 153 antiviral agents of the Pandemic Response Box that have inhibitory activity on cytopathic effect induced by EV-A71 infection in rhabdomyosarcoma (RD) cells.

3.2.2 To investigate the inhibitory effects of the selected drugs on the EV-A71 replication.

3.2 Hypothesis

Among 153 antiviral agents of the Pandemic Response Box that have been reported to elicit inhibitory effects on the related viruses contained in the compound library, they could be selected for the drugs that suppress EV-A71 replication by in vitro screening. The repurposed drugs might target the viral proteins that are conserved among closely related viruses and either the same or new cellular pathways that are essential for viral processes which leads to suppression of EV-A71 replication.

CHAPTER 4

RESEARCH METHODOLOGY

4.1 Experimental outline

Evaluation of cytotoxicity of 153 antiviral compounds of the MMV Pandemic Response Box to rhabdomyosarcoma (RD) cells by sulforhodamine B (SRB) assay.



Antivirals have negligible

In vitro screening of the antiviral drugs that have an inhibitory effect on cytopathic effect induced by EV-A71 infection.



Antivirals can rescue infected RD cells.

Investigation of inhibitory effects of the selected drugs on the EV-A71 replication by:

1. Quantifying intracellular EV-A71 RNA by quantitative real-time RT-PCR.
2. Determining viral protein synthesis by Western blot analysis reduction assay.
3. Quantifying release EV-A71 virions by median cell culture infectious dose (CCID50) assay.

4.2 Virus propagation

Objective: To propagate the EV-A71 and use it throughout this thesis. Rhabdomyosarcoma (RD) cells (JCRB9072) were purchased from the Japanese Collection of Research Bioresources Cell Bank and grown in Dulbecco's modified Eagle's medium (DMEM, Gibco, NY, USA) supplemented with 1 × GlutaMAX (Gibco, NY, USA), 10% heat-inactivated fetal bovine serum (HyClone, MA, USA), L-glutamine, and penicillin/streptomycin antibiotics (Gibco, NY, USA). The cells were incubated at 37 °C in the humidified air containing 5% CO₂. The viral stock of Thai clinical isolate of EV-A71 genotype B5 provided by Prof. Yong Poovorawan (Faculty of Medicine, Chulalongkorn University, Bangkok, Thailand) kept at -80 °C at the Molecular Immunology and Microbiology laboratory were propagated in 90-95% confluent cell monolayer of RD cells. The virus stock was diluted in a serum-free medium to prepare 0.1 multiplicity of infection (MOI) and incubated with the monolayer cells for 1 hour. The inoculum was aspirated. The cell monolayers were washed once with phosphate-buffered saline (PBS) and replenished with fresh DMEM. The infected cells that showed maximum cytopathic effect were subjected to repeat freeze-thaw 3 times to completely lyse the cells and release the virions to the culture medium. The cell homogenate was centrifuged to remove cellular debris. The cell lysate was harvested. The supernatant containing the virions was kept in small aliquots at -80 °C until use. The titers of the viral stock will be determined on a monolayer of RD cells according to the WHO Polio Laboratory Manual and calculated by Kärber formation expressed as the median cell culture infectious dose (CCID₅₀/100 µl).⁷⁸

4.3 Evaluation of cytotoxicity of 153 antiviral compounds of the MMV Pandemic Response Box to rhabdomyosarcoma (RD) cells by sulforhodamine B (SRB) assay

Objective: To screen antiviral drugs that have negligible cytotoxicity to RD cells.

4.3.1 Preparation of working antiviral compounds

The 153 antiviral compounds included in the drug library, MMV Pandemic Response Box, were supplied by the Medicines for Malaria Venture (MMV) in collaboration with the Drugs for Neglected Diseases *initiative* (DNDi).⁵⁶ The compound stocks (purity of > 90%) were prepared in 100% dimethyl sulfoxide (DMSO) (volume/volume) at 10 mM in 96-well plates. The compounds were renamed according to location in the plate layout of the Pandemic Response Box (plate-well number). To prepare 1 μ M working compounds, the compound stocks were 1:10,000 diluted in the completed DMEM. The working compounds were aliquoted and kept at $-80\text{ }^{\circ}\text{C}$ until further use. The 0.01% DMSO in the completed DMEM was used as a vehicle or negative control, namely DMSO.

4.3.2 Cytotoxicity assay

The percentage of cell survival of RD cells treated with compounds was assessed for cytotoxicity by SRB assay.⁷⁹ RD cell suspension was added in wells of a 96-well plate (10^4 cells per well). At 70% to 80% confluence, the RD cell monolayers were incubated with 1 μ M working antiviral compounds and kept for 24 hours to test the cytotoxicity of the compounds. Cell monolayers incubated with the completed DMEM and the 0.01% DMSO diluted in the completed DMEM served as maximum % cell survival and vehicle control, respectively. After incubation for 24 hours, the cell monolayers were fixed with 10% (% weight/ v) trichloroacetic acid and stained with sulforhodamine B (SRB) dye for 30 minutes. The excess dye was removed by washing with 1% (% v/v) acetic acid. The protein-bound SRB dyes were dissolved in 10 mM Tris base solution and the color intensity was determined by measuring absorbance at optical density (OD) at 510 nm using a FlashScan™ microplate reader (Thermo Fisher Scientific, Vantaa, Finland). The percentage of cell

survival was calculated by using the formula below. The cut-off was derived from the mean – 1 standard deviation (SD) value of % cell survival of the DMSO control group.

$$\% \text{ Cell survival} = \left[\frac{\text{OD}_{510\text{nm}} \text{ of test or irrelevant control}}{\text{OD}_{510\text{nm}} \text{ of maximum \% cell survival}} \right] \times 100$$

4.4 Screening of compounds with potential anti-EV-A71 activity

Objective: To screen antiviral drugs that can rescue RD cells infected with EV-A71.

To screen antiviral drugs that can rescue RD cells infected with EV-A71. The anti-EV-A71 activity is the ability to rescue the infected cells. The SRB assay was used to determine % of cells rescued from EV-A71-induced cytopathic effect (CPE) and was calculated for % cell survival relative to the maximum % cell survival control. The RD monolayer cells were infected with 1 MOI of EV-A71 as described in **Section 4.2** for 1 hour. After 1 hour, the inoculum was removed and replenished with a fresh culture medium containing 1 μM antiviral compounds as recommended by the MMV. The plates were incubated for 24 hours. Negative anti-EV-A71 activity control was the infected RD cell monolayers incubated with cell culture medium supplemented with DMSO, namely infDMSO. Maximum % cell survival and vehicle control were uninfected RD cells incubated with cell culture medium alone (DMEM) and DMSO, respectively. Given information provided by the MMV, positive anti-EV-A71 activity controls namely rupintrivir and T-1106 were two antiviral agents from plate D wells A7 (D-A7) and H7 (D-H7), respectively. They have been reported for potent anti-EV-A71 activity.^{54,55} Percentage cell survival was calculated as described in **Section 4.3**. The cut-off was % cell survival of positive control.

4.5 Dissecting mechanism of the inhibitory effect of the hit compounds on EV-A71 replication

Objective: To verify the inhibitory effects of the selected antiviral compounds on the EV- A71 replication cycle.

To verify the inhibitory effects of the selected antiviral compounds on the EV-A71 replication cycle. Virus reduction assays including reverse-transcription quantitative real-time PCR (qRT-PCR), Western blot analysis, and CCID₅₀ assay were performed to verify the anti-EV-A71 activity of the selected compounds. The qRT-PCR, Western blot analysis and CCID₅₀ assay quantified the intracellular viral RNA copy numbers, viral protein synthesis, and mature particle production, respectively. The RD cell monolayers were infected with EV-A71 at 1 MOI as described in **Section 4.2** for 1 hour. The infected RD cells were treated with 1 μ M compounds and incubated for 24 hours. The controls similar to **Section 4.4** including the positive anti-EV-A71 activity control, infDMSO, maximum % cell survival, and vehicle control were set in this experiment.

4.5.1 Sample preparation

At 24 hours post-treatment, cell culture supernatants were collected to perform the CCID₅₀ assay. The cell monolayers were washed once with sterile PBS. The total RNA and protein were extracted from the cell monolayers by adding 500 μ l Trizol reagent (Invitrogen) according to the manufacturer's instructions. The concentration of the prepared protein lysates was measured by Bradford protein assay. The concentration of the extracted RNA was determined by optical density (OD) at absorbance 260 nm measured by spectrophotometer (NanoDrop 2000/2000c, Thermo Fisher Scientific). The OD ratios of 260/280 nm and 260/230 nm greater than 1.8 and 2, respectively, were the high-quality genetic material of the extracted RNA. One microgram of total RNA of each sample was treated with DNase I following the instruction protocol, (Thermo Fisher Scientific). The RNA samples were diluted to 200 ng/ μ l and the fixed amounts of RNA were used in the qRT-PCR.

4.5.2 qRT-PCR

Recombinant pQE31 plasmids inserted with EV-A71 *VP1* coding sequence, namely pQE31::*VP1* constructed previously.⁸⁰, were 10-fold serially diluted to yield 10 to 10⁶ copies of the *VP1* for creating a standard curve. The formula used to calculate the number of *VP1* copies was the following.

$$\text{Number of copies} = \left[\frac{\text{Amount of plasmid (ng)} \times \text{Avogadro's number}}{\text{Length of dsDNA target } VP1 \text{ (bp)} \times \text{conversion factor} \times \text{mass of 1bp dsDNA}} \right]$$

$$\text{Number of copies} = \left[\frac{\text{Amount of plasmid (ng)} \times 6.022 \times 10^{23}}{409 \text{ (bp)} \times 10^9 \times 660} \right]$$

The one-step SYBR Green-based qRT-PCR reagents (Agilent, CA, USA) were mixed with the fixed amounts of RNA and pQE31::*VP1* as follows. The copy numbers of viral RNA were calculated from cycle threshold (Ct) values using the standard curve. Equations, namely $y=mx+b$, derived from the curve were used to calculate the *VP1* copies. The correlation between cycle threshold (Ct) values, the y-axis, and the number of *VP1* copies, the x-axis, was determined by R^2 . Y-axis interception, the b variable, indicates a limit of detection, the highest Ct. Slope, the m variable, was used to calculate the %PCR efficiency as the following formula. R^2 indicates how good one value is at predicting another. When R^2 is 1, the value of Y (Ct) can be used to accurately predict value of x. R^2 value > 0.99 provides good confidence in correlating two values. Ideally, the efficiency (E) of a PCR should be closely to 100%

$$\text{PCR efficiency ; E} \quad E = -1 + 10^{(-1/\text{slope})}$$

$$\text{\%PCR efficiency} \quad \%E = (E - 1) \times 100$$

Component	Volume/amount
EV-F2760 forward primer (10 μ M) (5'-ATGGKTATGYWAAYTGGGACAT-3')	1 μ L
EV-R3206 reverse primer (10 μ M) (5'-CCTGACRTGYTTMATCCTCAT-3')	1 μ L
RT-RNase block enzyme mixture	0.5 μ L
Brilliant II SYBR Green qRT-PCR Master Mix	6.25 μ L
Total RNA	200 ng
Nuclease-free water	Top up to 12.5 μ L
Total volume	4.5 μL

The thermal cycle consisted of the consecutive steps as follows.

Step	Temperature ($^{\circ}$ C)	Time
1. Reverse transcription	42	60 minutes
2. Initial denaturation	95	10 minutes
3. Thermocycling (40 cycles) of:		
Denaturation	95	30 seconds
Annealing	57	30 seconds
Extension	68	30 seconds
4. Melt curve analysis		

4.5.3 Western blot analysis

The protein lysates were subjected to Western blot analysis to measure EV-A71 capsid protein VP0 (VP2-VP4 precursor) levels as described previously.⁸¹ Beta-actin host proteins were determined and used as loading control and for comparison. Ten micrograms of protein lysates were separated by sodium dodecyl sulfate-polyacrylamide gel electrophoresis (SDS-PAGE). The SDS-PAGE gel was a denaturing discontinuous polyacrylamide gel consisting of two layers of 12% resolving gel and 4% stacking gel (Bio-Rad Laboratories). The separated proteins were transferred to nitrocellulose membranes (Bio-Rad Laboratories). The membranes were soaked in 5% (v/v) fetal bovine serum (FBS) diluted in PBS for 1 hour to block empty areas. The blotted membranes were washed with PBS containing 0.05% (v/v) Tween-20, namely PBS-T. After that, the membranes were separately incubated with 1:3,000 mouse anti-actin antibodies (cat. BF0198, Affinity Bio-sciences) and 1:3,000 mouse anti-enterovirus 71 antibodies (cat. 4175-0127, Bio-Rad Laboratories) for 1 hour. The membranes were washed and incubated with 1:3,000 goat anti-mouse IgG (H+L) conjugated with horseradish peroxidase (KPL, SeraCare) at room temperature for 1 hour. All antibodies were diluted in 0.2% FBS (v/v) in PBS-T. The membranes were incubated with Clarity Max Western ECL substrate (Bio-Rad Laboratories) at room temperature for 10 minutes. The ChemiDoc™ XRS+ (Bio-Rad Laboratories) was used to visualize and image the reactive protein bands. The protein levels of EV-A71 VP0 and β -actin were determined by measuring the protein band intensities using Image Lab™ Software (Bio-Rad Laboratories). The protein levels of EV-A71 VP0 were normalized with those of β -actin in each sample. The fold changes of normalized VP0 were relative to the infDMSO, a negative anti-EV-A71 activity control.⁸¹

4.5.4 CCID₅₀ assay

Cell culture supernatants were collected to perform the CCID₅₀ assay to determine titers of infectious EV-A71 virions.^{78,81} RD cells were suspended in the completed DMEM and plated at 100 µL with a seeding density of 1×10^4 cells/well of a 96-well plate. At 80% cell confluence, the RD cell monolayers were incubated with 100 µL of 10-fold serially diluted supernatants of the drug-treated group and controls. Each dilution of the supernatant samples was added in 8 replicate wells. The plates were incubated in a 5% CO₂ incubator. CPEs were observed daily for 3 days. The assay was terminated in which the maximum % cell survival controls reached a full confluence. The culture medium was aspirated from the wells. The cell monolayers were washed once with PBS and fixed with cold absolute methanol for 30 minutes at room temperature. The fixed cells were washed twice with PBS and stained with diluted Giemsa dye solution for 30 minutes at room temperature. The wells were rinsed gently with tap water and air-dried. The titer of the virus was calculated using the Kärber formula as follows.

$$\text{Log CCID}_{50} = L - [d (S - 0.5)]$$

where;

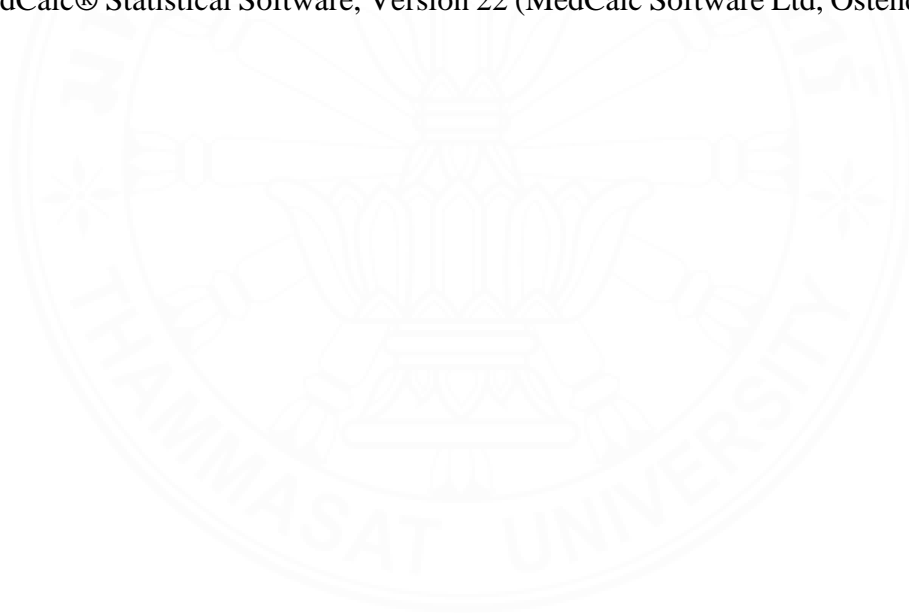
L = log of the lowest dilution used in the test

d = difference between log dilution steps

S = sum of the proportion of the positive test (i.e., cultures showing CPEs)

4.6 Statistical Analysis

The SRB assay and CCID₅₀ results were derived from three independent experiments. The qRT-PCR data were derived from technical triplicates of each sample conducted by three independent experiments. They were expressed in mean \pm standard deviations (SD). The mean \pm SD values of qRT-PCR and CCID₅₀ data of the antiviral-treated groups were compared with the infDMSO groups using one-way analysis of variance (one-way ANOVA) with Tukey-Kramer pair-wise comparison and independent samples t-test as necessary. The VP0 fold-change values were representative of two independent experiments. The A p-value less than 0.05 was taken to indicate a statistically significant difference. Statistical analysis was calculated by MedCalc® Statistical Software, Version 22 (MedCalc Software Ltd, Ostend, Belgium).



CHAPTER 5

RESULTS

5.1 Virus propagation

EV-A71 (Thai clinical isolate, genotype B5) designated as TUCU001/B5 isolate was successfully propagated in rhabdomyosarcoma (RD) cells. After 24 hours of infection, the infected cells initially showed explicit cytopathic effects (CPEs), the hallmarks of EV-A71 infection, including cell rounding, aggregation, and detachment. The CPEs increasingly occurred upon the time of infection and reached a maximum at day 3 post-infection. The clear wells were unstained cells that had full CPE positive (**Figure 5.1**). The strongly stained cells had less or no CPE. The proportions of the positive CPE wells were brought to calculate the CCID₅₀ by the Kärber formula. It was found that the propagated EV-A71 stock had a viral titer at $1 \times 10^{8.125}$ CCID₅₀/100 μ L.

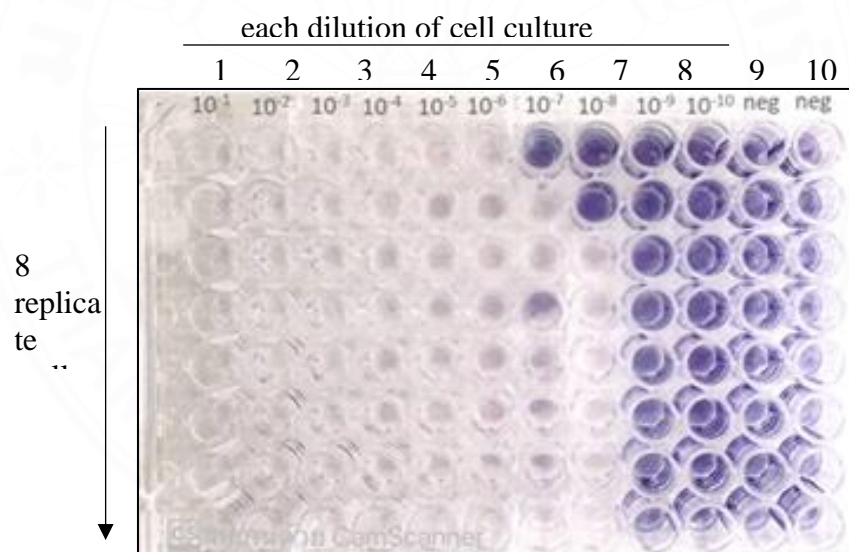
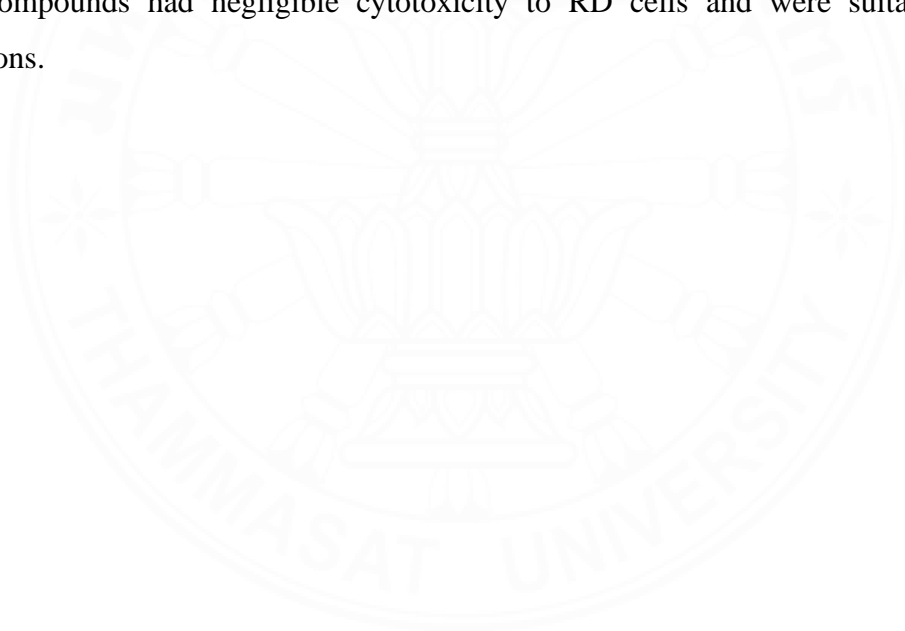


Figure 5.1 Determination of EV-A71 viral titer by cell culture infectious dose 50 (CCID₅₀). The digits 10^{-1} to 10^{-10} were dilutions of the cell culture supernatant. On columns 1 to 10, each dilution of the supernatant was added in 8 replicate wells. Columns 11 and 12 were negative infection control.

5.2 Evaluation of Cytotoxicity of Antiviral Compounds of the MMV Pandemic Response Box

The cytotoxicity of the 153 antiviral agents at 1 μ M was tested with rhabdomyosarcoma (RD) cell monolayers. The percentage of cell survival of RD cells treated with compounds was assessed for cytotoxicity by SRB assay. Maximum % cell survival and vehicle control were RD cells incubated with culture medium alone (DMEM) and supplemented with dimethyl sulfoxide (DMSO), respectively. It was found that the DMEM and DMSO controls had 100 ± 4.83 % and 96.31 ± 10.74 % cell survival, respectively (**Figure 5.2**). The cut-off was derived from the mean – 1 standard deviation (SD) value of % cell survival of the DMSO control group which is approximately 85%. There were 18 of 153 antiviral agents that had % cell survival higher than the cut-off ranging from 86.68 ± 7.76 to 201.07 ± 25.86 . It was suggested that the selected 18 antiviral compounds had negligible cytotoxicity to RD cells and were suitable for further investigations.



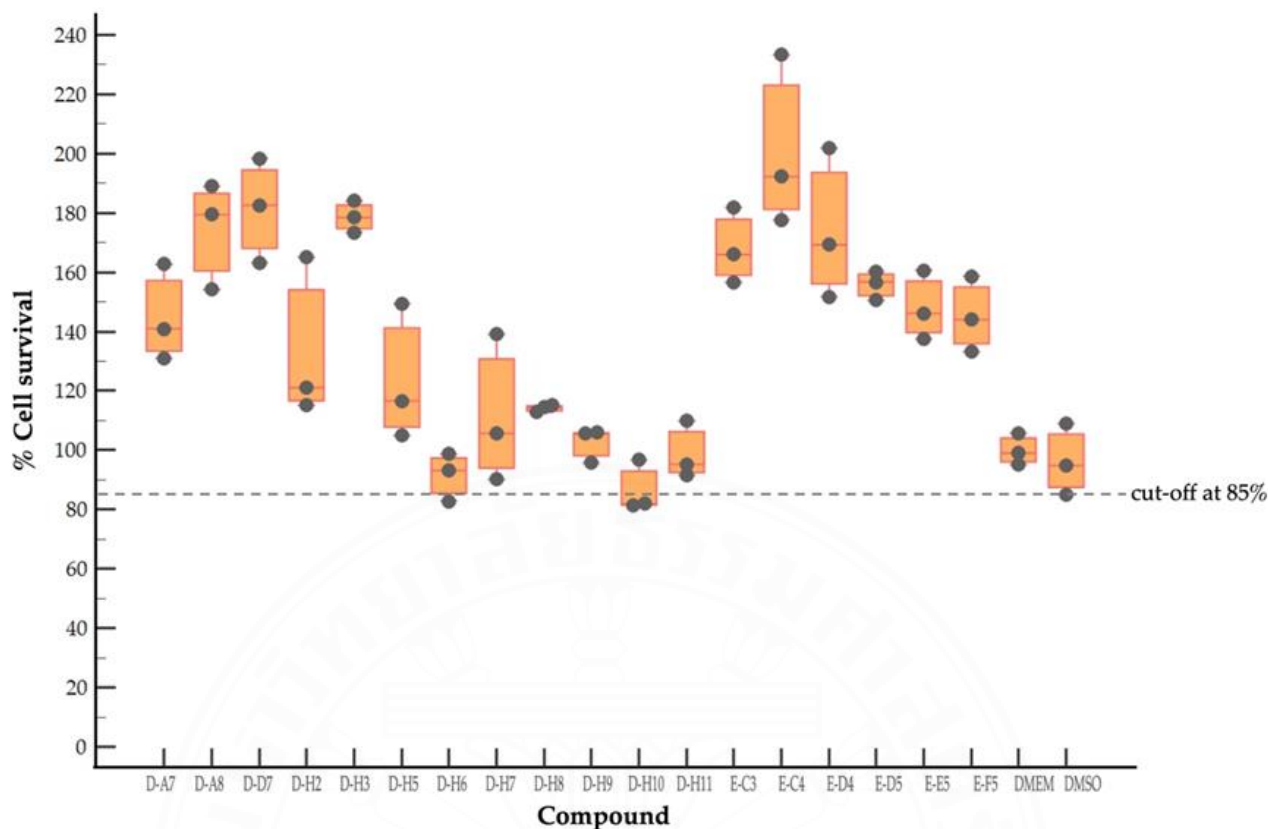


Figure 5.2 Cytotoxicity of Antiviral Compounds of the MMV Pandemic Response Box. Percentage of cell survival of RD cells treated with 18 antiviral compounds in the Pandemic Response Box that had negligible cytotoxicity. In this thesis, the compounds were renamed according to location in the plate layout of the Pandemic Response Box (plate-well number). After 24 hours, the cytotoxicity was determined by a sulforhodamine B (SRB) assay. DMEM and DMSO were cell culture medium alone and supplemented with DMSO were maximum % cell survival and vehicle control, respectively. The % cell survival was relative to the maximum % cell survival control. The % cell survival values are derived from three independent experiments and presented in Box-and-whisker and dot plots. Each dark grey circle represents the individual data points. The middle bar is the median and the boxes represent quartile data distribution. The dashed line represents the cut-off point derived from a mean – 1SD of % cell survival of the DMSO controls.

5.3 Screening of Compounds with Potential Anti-EV-A71 Activity

The 18 antiviral compounds in the Pandemic Response Box that had negligible cytotoxicity were determined for anti-EV-A71 activity by rescuing the infected RD cells. After 1 hour, the inoculum was removed and replenished with a fresh culture medium containing 1 μ M antiviral compounds as recommended by the MMV. After 24 hours, the ability of the tested antivirals to rescue the infected cells was determined by % cell survival compared to the maximum % cell survival control. The results showed that the infDMSO, the negative anti-EV-A71 activity control, showed 61.77 ± 8.44 % cell survival compared to the uninfected cells (**Figure 5.3**). Moreover, among positive anti-EV-A71 activity controls, the D-H7 (T-1106) exerted $71.18\% \pm 6.13$ cell survival which was higher than those of D-A7 (rupintrivir), i.e. $67.36\% \pm 4.7$. Therefore, the cut-off point was set to 71.18 according to the D-H7 (T-1106). Because the detailed mechanism of the T-1106 on EV-A71 replication has not been elucidated, it was included in the subsequent experiment as a hit compound. The EV-A71 infected-RD cells treated with the D-D7 compound had 92.99 ± 5.94 % cell survival. While those of D-H2, D-H7, D-H8, E-C3, E-C4, and E-E5 range from $70.61\% \pm 1.42$ to $77.77\% \pm 3.36$. It was suggested that the seven hit compounds might potentially have anti-EV-A71 activity as they can rescue the infected cells. They were investigated further for the inhibitory effects on EV-A71 replication. Characteristics of those hit compounds are described in **Table 5.1**

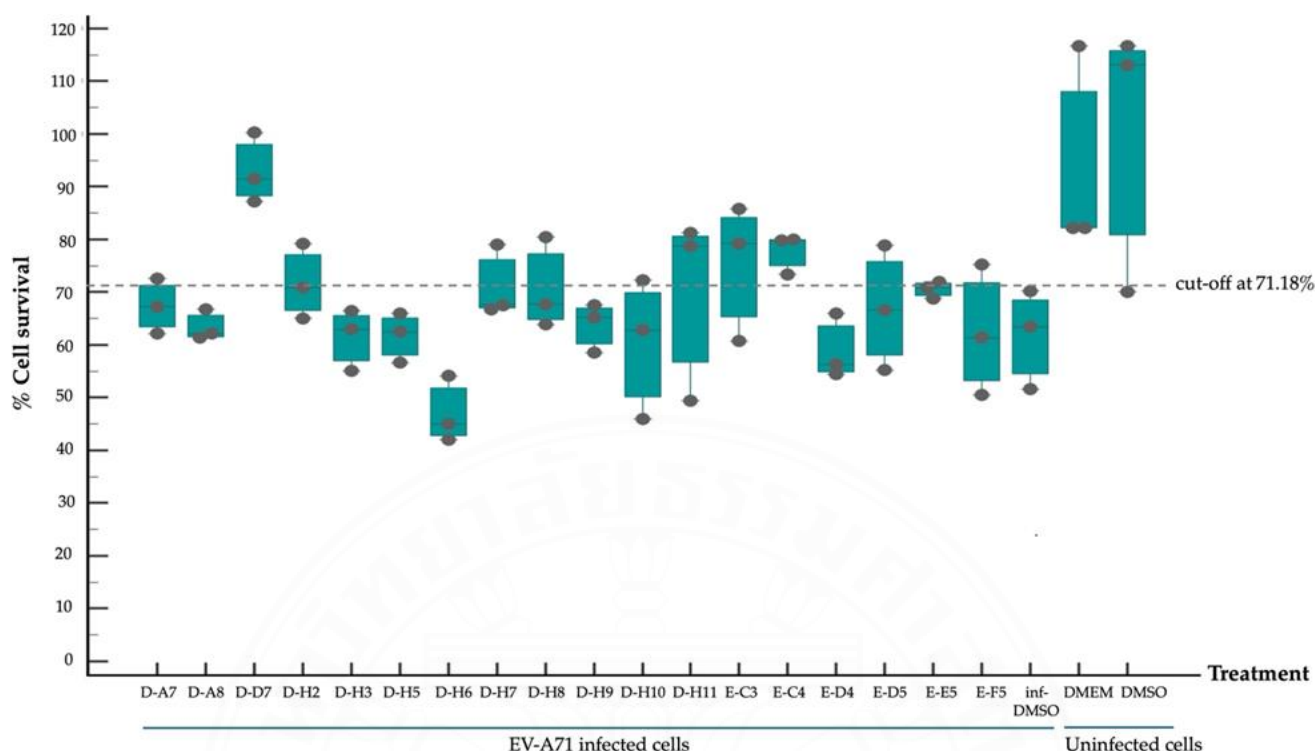


Figure 5.3 Compounds with Potential Anti-EV-A71 Activity. There were seven hit compounds including D-D7, D-H2, D-H7, D-H8, E-C3, E-C4, and E-E5 that had potential anti-EV-A71 activity. The infDMSO served as negative anti-EV-A71 activity control. Given the information by the MMV, the D-A7 (rupintrivir) and D-H7 (T-1106) compounds served as positive anti-EV-A71 activity control. Uninfected RD cells incubated with cell culture medium alone (DMEM) and DMSO served as maximum % cell survival and vehicle control, respectively. The % cell survival values are derived from three independent experiments and presented in Box-and-whisker and dot plots as described in **Figure 5.2**. The dashed line represents the cut-off point relative to the positive anti-EV-A71 activity control (D-H7).

Table 5.1. Chemical structures, alternative names, and mode of action of the selected hit compounds.

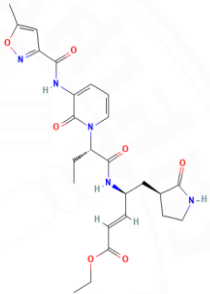
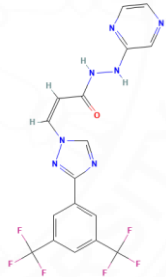
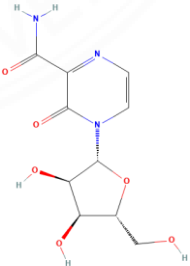
Compound (MMV ID)	ChEMBL ID	Trivial name	Formula	Structure	Mode of action
D-D7 (MMV1782112)	CHEMBL 141816	2-pyridone- containing human rhinovirus 3C protease inhibitor ⁽³⁵⁾	C ₂₅ H ₃₁ N ₅ O ₇		Polypeptide processing inhibitor of human rhinovirus 3C protease (35).
D-H2 (MMV1593517)	CHEMBL 3545185	Selinexor ⁽⁵⁸⁾	C ₁₇ H ₁₁ F ₆ N ₇ O		Nuclear export protein inhibitor of CRM1 or XPO1 ⁽⁵⁸⁾ .
D-H7 (MMV1782104)	CHEMBL 261459	T-1106 ⁽⁵⁹⁾	C ₁₀ H ₁₃ N ₃ O ₆		RNA polymerase inhibitor of EV-A71 ⁽⁵⁹⁾ .

Table 5.1. Chemical structures, alternative names, and mode of action of the selected hit compounds. (Cont.)

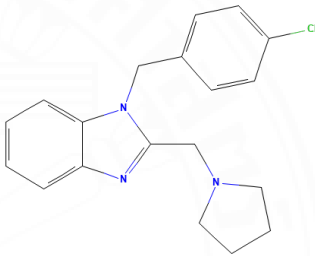
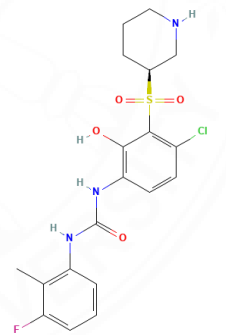
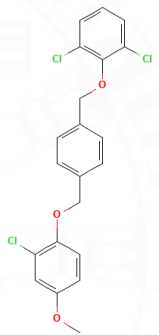
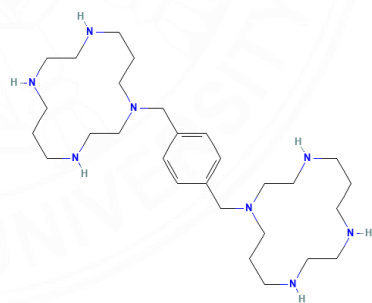
Compound (MMV ID)	ChEMBL ID	Trivial name	Formula	Structure	Mode of action
D-H8 (MMV002015)	CHEMBL 1407943	Clemizole ⁽⁶⁰⁾	C ₁₉ H ₂₀ ClN ₃		NS4B protease inhibitor of HCV ⁽⁶⁰⁾
E-C3 (MMV1581034)	CHEMBL 3039531	Danirixin ⁽⁶⁴⁾	C ₁₉ H ₂₁ ClFN ₃ O ₄ S		Reversible antagonist of CXCR2 chemokine receptor ⁽⁶⁴⁾

Table 5.1. Chemical structures, alternative names, and mode of action of the selected hit compounds. (Cont.)

Compound (MMV ID)	ChEMBL ID	Trivial name	Formula	Structure	Mode of action
E-C4 (MMV1580485)	CHEMBL 1235858	Pocapavir ⁽⁶⁵⁾	C ₂₁ H ₁₇ Cl ₃ O ₃		Viral capsid inhibitor of enteroviruses ⁽⁶⁵⁾
E-E5 (MMV1580502)	CHEMBL 18442	Plerixafor ⁽⁶⁶⁾	C ₂₈ H ₅₄ N ₈		CXCR4 chemokine receptor antagonists ⁽⁶⁶⁾

5.4 Dissecting Mechanism of Inhibitory Effect of the Hit Compounds on EV- A71 Replication

The inhibitory effect of the D-D7, D-H2, D-H7, D-H8, E-C3, E-C4, and E-E5 compounds on the EV-A71 replication cycle was investigated in the infected-RD cells. The infDMSO, infected cells incubated with a cell culture medium supplemented with DMSO, were used as negative inhibition control and for comparison. The level of genome replication was quantified in the intracellular EV-A71 RNA by qRT-PCR using a standard curve constructed from known amounts of recombinant plasmids inserted with EV-A71 *VP1* coding sequence. Levels of viral protein synthesis were measuring the EV-A71 unprocessed VP2-VP4 precursor protein, namely VP0, by Western blot analysis and densitometry. The calculated VP0 protein levels were compared with the infDMSO control and expressed as fold-change. The release virions of EV-A71 were determined by CCID₅₀ assay.

The standard curves were constructed from the recombinant pQE31 plasmids inserted with EV-A71 *VP1* coding sequence by 10-fold serially diluting the plasmids to yield 10 to 10⁶ copies of the *VP1*. The standard curves were individually constructed for each independent experiment. A representative standard curve is shown in **Figure 5.4**. It showed that the expected *VP1* copies had a good correlation with the cycle threshold (Ct) values as R^2 was 0.991. The calculated % PCR efficiency was 105.03%. The Ct at 34.30 was a limit of detection. These parameters indicate the good reliability of the standard curve.

Among seven compounds, only D-D7, D-H2, and D-H7 exhibited significant suppression of replication of the EV-A71 viral genome at approximately 5-log, 1-log, and 1-log reduction of copy numbers of intracellular viral RNA level, respectively (**Figure 5.5A**). The E-C3, E-C4, and E-E5 compounds significantly increased approximately 1-log increment of EV-A71 RNA copy numbers (**Figure 5.5B**). It was found that the EV-A71 protein synthesis was reduced significantly by the D-D7 and E-C4 compounds, but marginally by the remaining five compounds (**Figure**

5.5). Only the D-D7 compound could suppress the production of infectious EV-A71 particles at approximately a 5-log reduction of CCID50 (**Figure 5.6**).

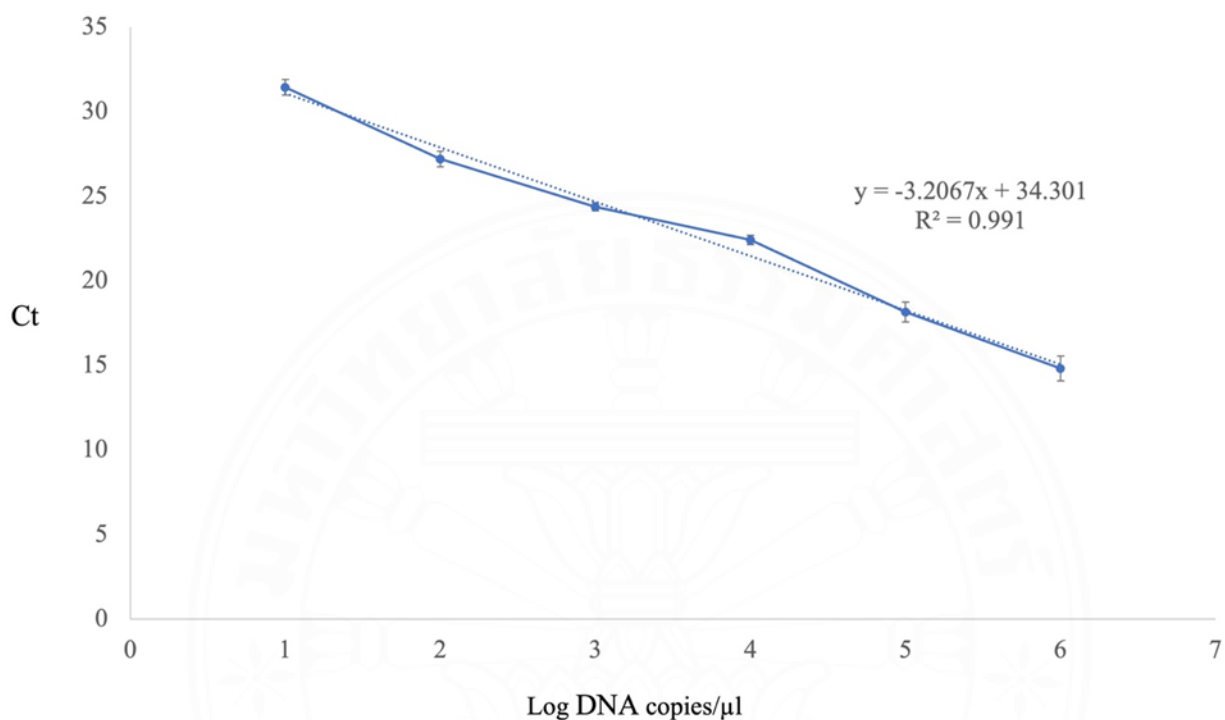


Figure 5.4 A representative standard curve of *VPI* used to calculate EV-A71 RNA number copies. Equations, namely $y=mx+b$ derived from the curve were used to calculate the *VPI* copies. The correlation between cycle threshold (Ct) values, the y-axis, and the number of *VPI* copies, the x-axis, was determined by R^2 . Y-axis interception, the b variable, indicates a limit of detection, the highest Ct. Slope, the m variable, was used to calculate the % PCR efficiency. Slopes between -3.1 and -3.6 giving reaction efficiencies between 90 and 110% are typically acceptable. The log10 EV-A71 RNA copy numbers are the means derived from the technical triplicates of each sample. Error bars represent standard deviations.

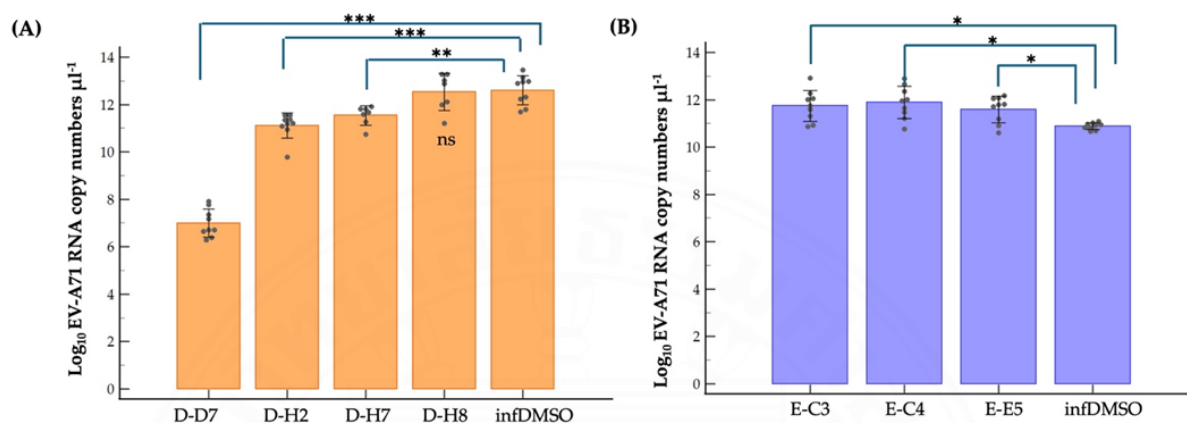


Figure 5.5 Anti-EV-A71 activity by virus reduction assays for viral RNA copy numbers using qRT-PCR. The hit compounds D-D7, D-H2, D-H7, and D-H8 (**A**) and E-C3, E-C4, and E-E5 (**B**) were verified for anti-EV-A71 activity by virus reduction assays for viral RNA copy numbers using qRT-PCR and standard curves. The log₁₀ EV-A71 RNA copy numbers μl⁻¹ values are the means of three independent experiments. Error bars represent standard deviations. Each dark grey circle represents the individual data points. *, **, and *** represent a statistically significance difference at p-value < 0.05, p-value < 0.001, and p-value < 0.0001, respectively. ns indicates no significance.

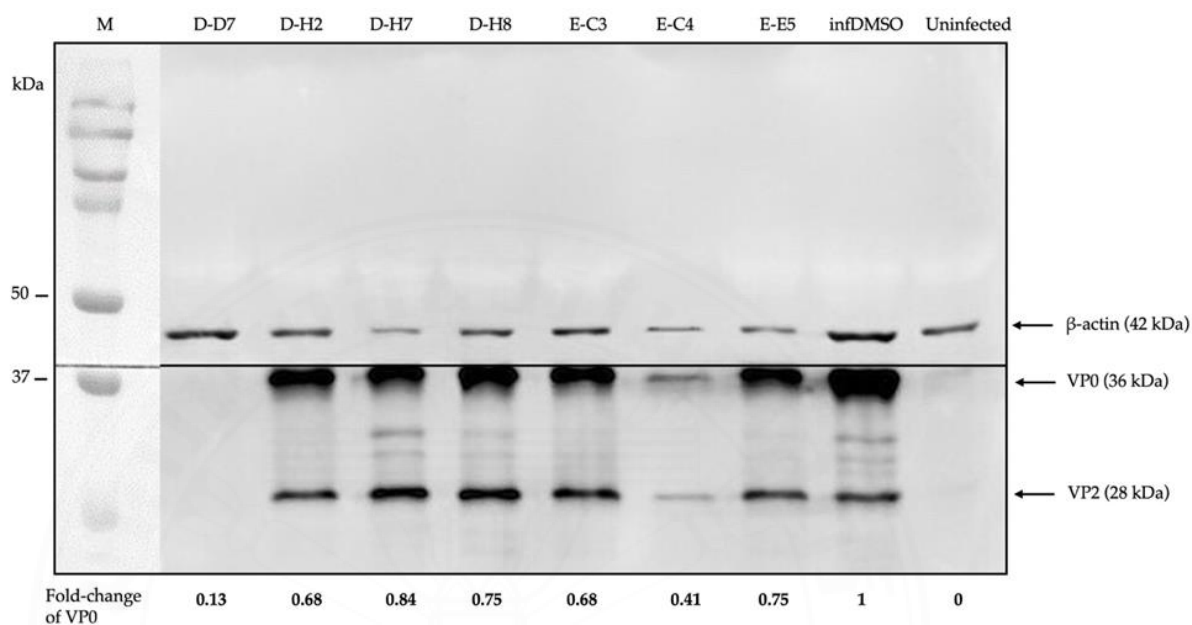


Figure 5.6 Anti-EV-A71 activity by virus reduction assays for viral protein synthesis using Western blot analysis and densitometry. The hit compounds D-D7, D-H2, D-H7, D-H8, E-C3, E-C4, and E-E5 were verified for anti-EV-A71 activity by virus reduction assays for viral protein synthesis using Western blot analysis and densitometry. The VP0 fold-change values are representative of two independent experiments. Lane M is a protein marker. Beta-actin bands are used for protein normalization and internal loading control.

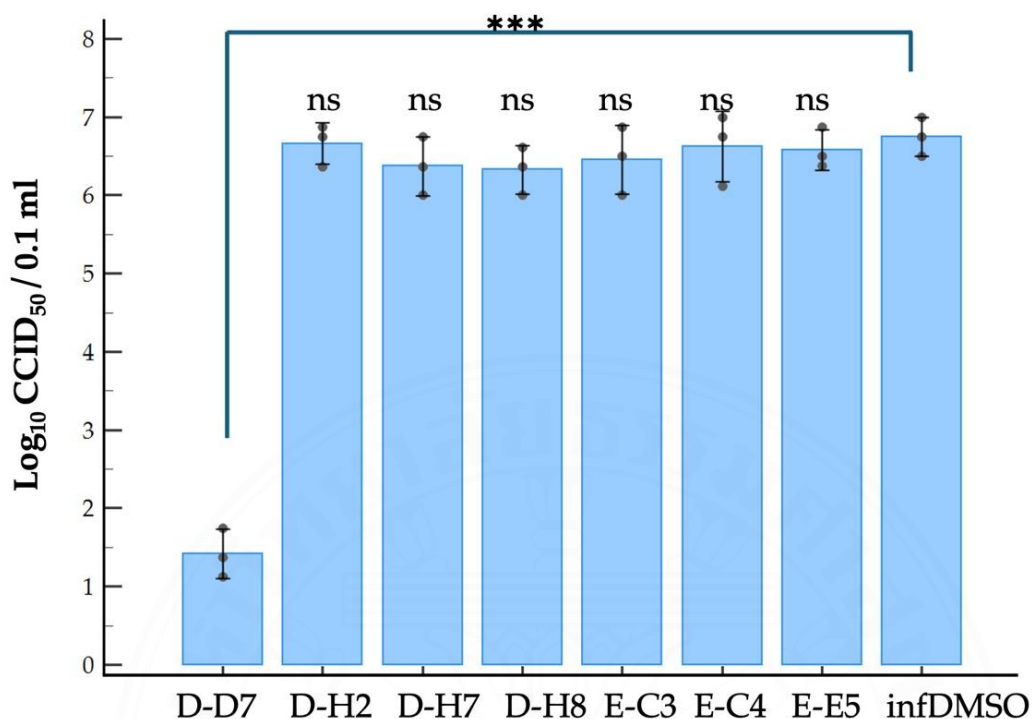


Figure 5.7 Anti-EV-A71 activity by virus reduction assays for the release of EV-A71 virions using CCID₅₀ assay. The hit compounds D-D7, D-H2, D-H7, D-H8, E-C3, E-C4, and E-E5 were verified for anti-EV-A71 activity by virus reduction assays for the release of EV-A71 virions using CCID₅₀ assay. The log₁₀ CCID₅₀ / 0.1 ml values are the means of three independent experiments. Error bars represent standard deviations. Each dark grey circle represents the individual data points. *** represents a statistically significance difference at p-value < 0.0001. ns indicates no significance.

CHAPTER 6

DISCUSSION

By screening the antivirals in the Pandemic Responses Box drugs library, seven hit compounds including 2-pyridone-containing peptidomimetics (D-D7), Selinexor (D-H2), T-1106 (D-H7), Clemizole (D-H8), Danirixin (E-C3), Pocapavir (E-C4), and Plerixafor (E-E5) were identified to have both negligible cytotoxicity towards RD cells and potential anti-EV71 activity. Some of them had inhibitory effects on reducing EV-A71 genome replication and protein synthesis. The 2-pyridone-containing peptidomimetics exhibited the highest anti-EV71 activity affecting viral RNA replication, viral protein synthesis, and viral release steps of the replication cycle

The enteroviral 3C proteases play an indispensable role in the viral replication cycle by cleaving the nascent polyprotein to generate functional viral proteins.^{35,71} The functional viral proteins of enteroviruses facilitate an effective replication cycle by interacting with diverse host molecules and cellular pathways. Importantly, the catalytic motif Gly-X-Cys/Ser-Gly-Gly is structurally conserved in picornaviral 3C proteases and serine proteases.⁷¹ Hence, they have been the ideal target for pan-picornavirus antiviral.⁷¹ In this thesis, the 2-pyridone-containing peptidomimetics (D-D7), which has an original mode of action for polyprotein processing inhibitor of human rhinovirus (HRV) 3C protease, could be repurposed towards EV-A71. To explain the mechanism of anti-EV-A71 activity, the similarity of the architecture of substrate binding cleft and mechanisms for substrate recognition between 3C proteases of HRV and EV-A71 were searched from the literature review.^{35,71} It was found that the substrate-binding cleft of EV-A71 3C could be superimposed on those of HRV 3C upon substrate binding as shown in **Figure 6.1**.⁷¹

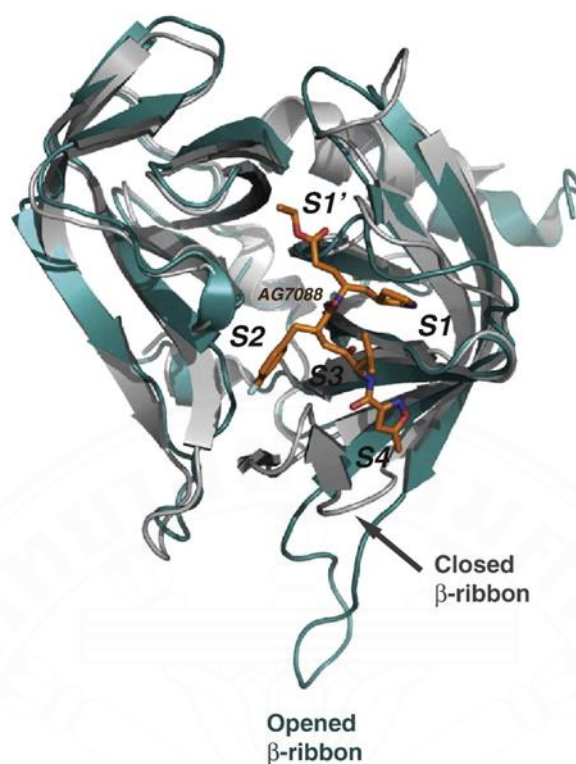


Figure 6.1 Superimposition of EV-A71 3C and HRV 3C–AG7088 structures. The deep teal ribbon model is an EV-A71 3C structure. The complex of HRV 3C–AG7088 structures are gray ribbon and orange elements, respectively. AG7088 or Rupintrivir is a 3C inhibitor bound at substrate-binding pockets, S1'–S4.⁷¹

In **Figure 6.2**, the crystal structure analysis reveals the formation of an irreversible covalent bond between the 2-pyridone-containing peptidomimetics (D-D7) and the active site cysteine residue of HRV 3C, namely Cys147.³⁵ This Cys147 residue is conserved among 3C proteins of picornaviruses including EV-A71 and HRV (**Figure 6.3**).⁷¹ Taken together, the 2-pyridone-containing peptidomimetics can potentially bind the active site of EV-A71 3C protease. Therefore, the anti-EV-A71 activity of the 2-pyridone-containing peptidomimetic is likely an EV-A71 3C protease inhibitor. Given functions at the early step of viral replication, interference of 3C protease by the 2-pyridone-containing peptidomimetics (D-D7) results in a drastic reduction of intracellular EV-A71 viral RNA, viral protein synthesis, and new virions. EV-A71 3C protein is a 183 amino acid cysteine protease. It has a diverse function to promote viral replication including cleaving viral polyprotein, interfering apoptosis regulation, and subverting the innate immune system.¹⁶ Hence, it could be expected that the 2-pyridone-containing peptidomimetics (D-D7) not suppress EV-A71 replication only but also restores the altered cellular pathways upon the infection. This study has highlighted the 2-pyridone-containing peptidomimetics to be a potent anti-EV-A71 drug. These inconclusive mechanisms warrant further experimental validations.

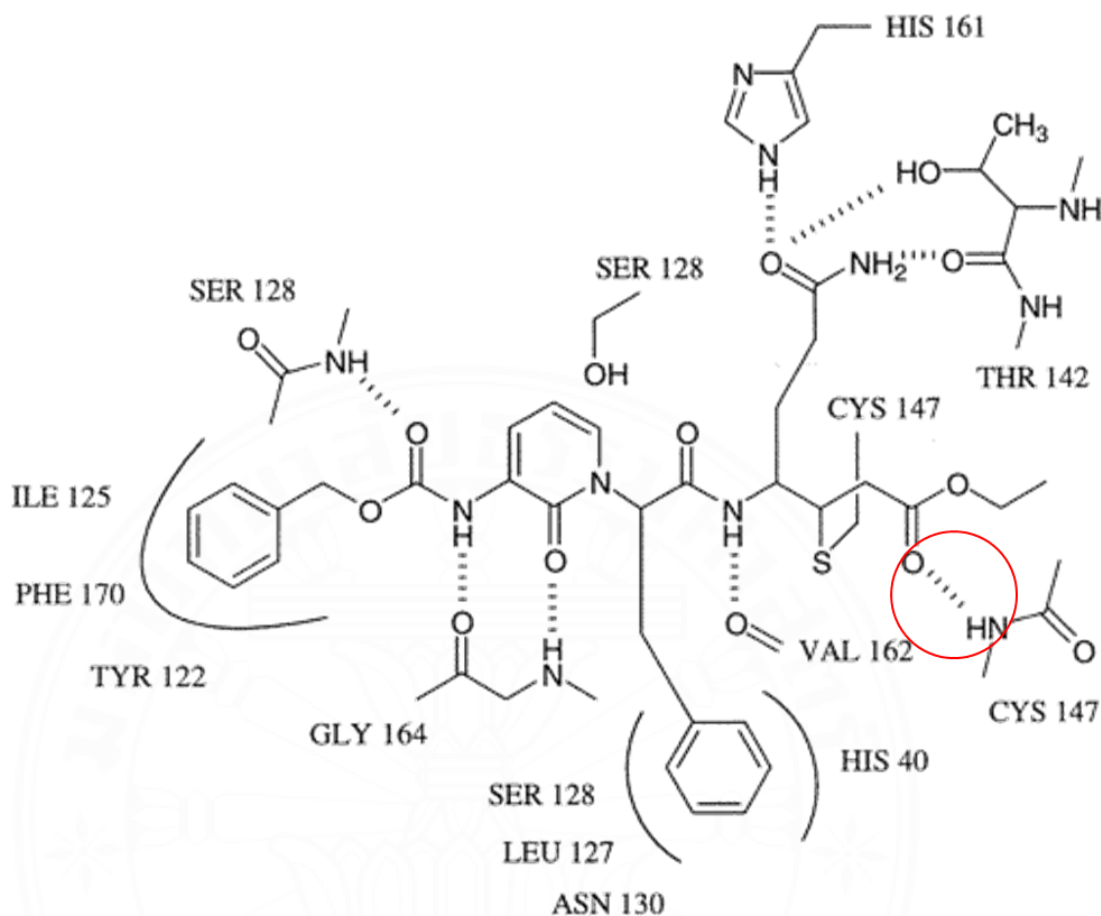


Figure 6.2 Schematic diagram of the crystal structure of HRV 3C complexed with the 2-pyridone-containing peptidomimetics.³⁵ Dashed lines represent hydrogen bonds and the residues constituting the enzyme binding subsites including the Cys147. A covalent bond (in the red circle) is observed between the active site Cys147 and the β -carbon of the Michael acceptor of the 2-pyridone-containing peptidomimetics.

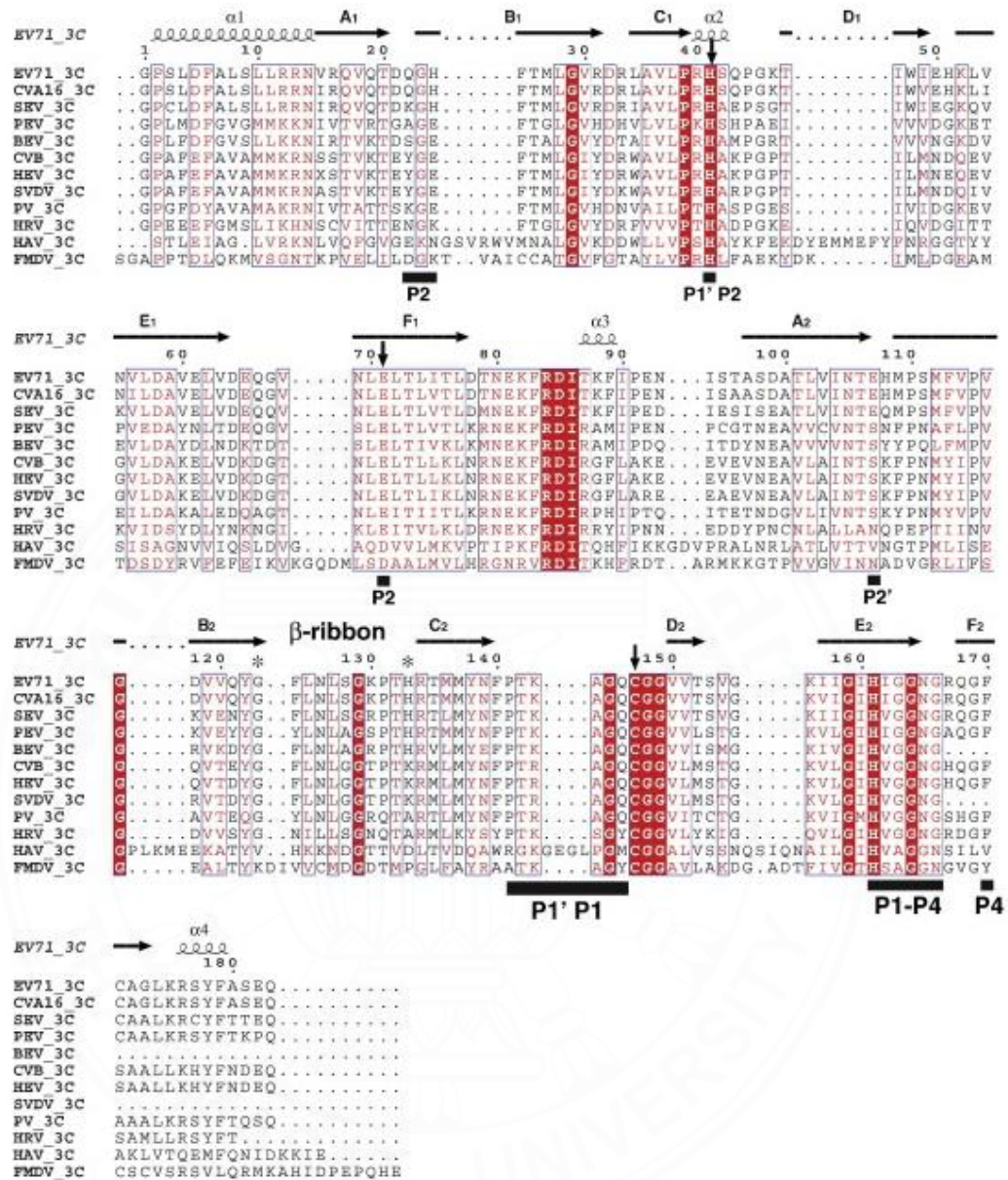


Figure 6.3 Structure-based multiple-sequence alignment of 3C proteases of different picornaviruses. The secondary structure is shown on top of the multiple-sequence alignment. Invariant residues in picornaviral 3C are highlighted with a red background. The conserved residues are shown in red letters. Black bars at the bottom of the sequence indicate residues directly involved in substrate binding. The catalytic triads, His40, Glu71, and Cys147, in the active site of EV71 3C, are indicated by black descending arrows.⁷¹

Selinexor is an inhibitor of nuclear export protein exportin-1 (XPO1).⁸² Selinexor in combination with dexamethasone has been FDA-approved to treat multiple myeloma.⁸² Anti-SARS-CoV-2 activity of Selinexor has been reported to inhibit the nuclear export of ORF3b, ORF9b, and nucleocapsid viral proteins and ACE-2 host receptors leading to suppression of the virus replication.⁷³ Given the nuclear export, the genome of EV-A71 requires ITAFs to interact with IRES and drive cap-independent translation. Hence, Selinexor might interfere with the nuclear export of some ITAFs interacting with EV-A71 IRES resulting in a slight reduction of viral protein synthesis and intracellular viral RNA. However, Selinexor treatment did not affect the production of new virions. Selinexor not only interferes with nuclear export but also downregulates pro-inflammatory cytokines commonly associated with the cytokine storm observed in COVID-19 patients.⁷³ Regarding immunopathogenesis of EV-A71 infection, the modulation of inflammation in EV-A71 infected cells by Selinexor should be investigated.⁸³

T-1106 is a nucleoside analog version of favipiravir lacking fluorine.⁷⁴ T-1106 can be metabolized to triphosphate yielding a drug with efficacy better than favipiravir.⁷⁴ General nucleoside analogs, once incorporated into the viral genome, induce lethal mutagenesis or chain termination.⁵⁵ The T-1106, once incorporated into the EV-A71 genome by the RdRp enzyme, causes the RdRp to pause and backtrack, promoting template switching and the formation of defective viral genomes. It has been reported that T-1106 could inhibit EV-A71 replication in RD cells requiring very high concentrations between 200 μ M and 600 μ M.⁵⁵ This thesis used only 1 μ M T-1106 to treat EV-A71-infected RD cells. Therefore, it could slightly suppress EV-A71 RNA replication and protein synthesis which insufficiently affects virion production

Pocapavir is an enterovirus-specific capsid inhibitor.³³ It has been used as an investigational drug for the treatment of coxsackievirus and echovirus 11.^{75,76} It has been reported for clearance of vaccine-derived type 3 poliovirus infection in an infant with underlying X-linked agammaglobulinemia.⁷⁷ The binding site of Pocapavir is within the pocket located in the structural protein VP1, namely canyon.⁶⁸ The Pocapavir binding causes increased stability of the viral capsid, thus preventing conformational changes necessary for receptor interaction and uncoating. It acts in the early stages of

the enterovirus replication cycle. Related papers demonstrated that EV-A71 genome uncoating was initiated at 20 minutes post-infection in RD cells followed by an increase of intracellular viral RNA at 2 hours post-infection.⁸⁵ The virus secretion was detected at 8 hours post-infection. In this thesis, the EV-A71-infected RD cells were added with Pocapavir at 1-hour post-infection, in which the viruses might be completed for receptor binding and genome uncoating stages already. Hence, the binding sites of Pocapavir are already occupied by receptor engagement. Therefore, it did not affect virion production in our model. Our study demonstrated that Pocapavir significantly suppressed VP0 synthesis. The VP0 (precursor of VP2 and VP4) does not contain the inhibitor-binding site. Hence, it could be postulated that Pocapavir might interfere with the biogenesis of intracellular EV-A71 capsid protein.

Clemizole, Danirixin, and Plerixafor showed only a slight interference effect on the VP0 protein level. They did not exhibit anti-EV-A71 activity. Hence, they might interfere with host factors involving the biogenesis of intracellular EV-A71 capsid protein.

Interestingly, Danirixin, Pocapavir, and Plerixafor could enhance EV-A71 RNA levels in the infected RD cells. It has been reported that intracellular EV-A71 VP1 could induce autophagy to regulate viral replication.⁸⁶ Hence, it could be hypothesized that the Pocapavir might interact with intracellular VP1 and enhance VP1-induced autophagy activity. Danirixin and Plerixafor are antagonists of CXCR2 and CXCR4 chemokine receptors, respectively. They are G protein-coupled receptors (GPCR) involving several downstream signaling pathways that facilitate various tissue-dependent signals including cell migration, adhesion, proliferation, survival, and differentiation.^{87,88} It has been reported that CXCR2 and CXCR4 engaging with cognate cytokines can induce apoptosis.^{88,89} EV-A71 can regulate apoptosis for the benefit of its replication.⁹⁰ Hence, in this thesis, it was speculated that Danirixin and Plerixafor could enhance EV-A71 RNA replication upon binding with their cognate chemokine receptor antagonists and suppress apoptosis.

Besides the effects of the hit compounds, the EV-A71 might possess compensatory mechanisms to involve the abovementioned phenomena. Those inconclusive mechanisms warrant further investigations.

CHAPTER 7

CONCLUSION

The novel anti-EV-A41 antivirals could be successfully discovered from the MMV Pandemic Response Box drug library by *in vitro* screening of 153 antiviral agents using a cell-based model. The 2-pyridone-containing peptidomimetic originally inhibits HRV 3C protease and can be repurposed towards EV-A71 antiviral. The 3C inhibitor drastically reduces viral replication. The 3C protease inhibitor binds a conserved residue Cys147 of the catalytic motif. Because of the structure and sequence similarity of 3C proteases among the closely related viruses, the 2-pyridone-containing peptidomimetic is potentially pan-picornavirus antiviral. T-1106, a nucleoside analog modified from Favipiravir antiviral, and Selinexor, a nuclear export inhibitor, have a promising anti-EV-A71 activity to suppress the synthesis of viral RNA and protein. Pocapavir, an enterovirus-specific capsid inhibitor, is likely ineffective in the post-infection model of EV-A71. The rapid dynamics of viral replication could compromise the anti-EV-A71 activity of the capsid inhibitor. However, Pocapavir could interfere with the biogenesis of EV-A71 capsid protein. Clemizole, Danirixin, and Plerixafor might interfere with host molecules or pathways involving the EV-A71 replication cycle. The seven hit compounds discovered by this thesis warrant further characterization and development.

REFERENCES

1. Koh WM, Badaruddin H, La H, Chen MI-Cheng, Cook AR. Severity and burden of hand, foot and mouth disease in Asia: a modelling study. *BMJ Global Health*. 2018;3(1):e000442.
2. Sabanathan S, Tan LV, Thwaites L, Wills B, Qui PT, Rogier van Doorn H. Enterovirus 71 related severe hand, foot and mouth disease outbreaks in South-East Asia: current situation and ongoing challenges. *J Biomed Sci*. 2014;68(6):500–2.
3. Mercorelli B, Palù G, Loregian A. Drug Repurposing for Viral Infectious Diseases: How Far Are We? *Trends in Microbiology*. 2018;26(10):865–76.
4. Li X, Peng T. Strategy, Progress, and Challenges of Drug Repurposing for Efficient Antiviral Discovery. *Frontiers in Pharmacology*. 2021;12:660710.
5. Huang SW, Cheng D, Wang JR. Enterovirus A71: virulence, antigenicity, and genetic evolution over the years. *J Biomed Sci*. 2019;26:81.
6. Yang S, Li P, Li Y, Li W, Lai W, Zhu C, et al. Clinical manifestations of severe enterovirus 71 infection and early assessment in a Southern China population. *J Biomed Sci*. 2017;17(1):153.
7. Chang YK, Chen KH, Chen KT. Hand, foot and mouth disease and herpangina caused by enterovirus A71 infections: a review of enterovirus A71 molecular epidemiology, pathogenesis, and current vaccine development. *Revista IMT*. 2018;60:70.
8. Feng M, Liao Y, Gao Y, Jiang G, Wang L, Zhang Y, et al. Mechanism for the lethal effect of enterovirus A71 intracerebral injection in neonatal mice. *Lab Invest*. 2020;100(4):596–605.
9. Kobayashi K, Koike S. Cellular receptors for enterovirus A71. *J Biomed Sci*. 2020;27(1):23.
10. Lee KY. Enterovirus 71 infection and neurological complications. *Korean Journal of Pediatrics*. 2016;59(10):395.
11. Jin Y, Zhang R, Wu W, Duan G. Antiviral and Inflammatory Cellular Signaling Associated with Enterovirus 71 Infection. *Viruses*. 2018;10(4):155.

12. Chen CS, Yao YC, Lin SC, Lee YP, Wang YF, Wang JR, et al. Retrograde Axonal Transport: a Major Transmission Route of Enterovirus 71 in Mice. *J Viral*. 2007;81(17):8996–9003.
13. Hsia SH, Lin JJ, Chan OW, Lin TY. Cardiopulmonary failure in children infected with Enterovirus A71. *J Biomed Sci*. 2020;27(1):5.
14. Chang LY, Lin HY, Gau SSF, Lu CY, Hsia SH, Huang YC, et al. Enterovirus A71 neurologic complications and long-term sequelae. *J Biomed Sci*. 2019;26(1):57.
15. Chang CS, Liao CC, Liou AT, Chang YS, Chang YT, Tzeng BH, et al. Enterovirus 71 targets the cardiopulmonary system in a robust oral infection mouse model. *Sci Rep*. 2019;9(26):93.
16. Yuan J, Shen L, Wu J, Zou X, Gu J, Chen J, et al. Enterovirus A71 Proteins: Structure and Function. *Frontiers in Microbiology*. 2018;9:286.
17. Lai MC, Chen HH, Xu P, Robert. Translation control of Enterovirus A71 gene expression. *J Biomed Sci*. 2020;27(1):22.
18. Huang SW, Cheng D, Wang JR. Enterovirus A71: virulence, antigenicity, and genetic evolution over the years. *J Biomed Sci*. 2019;26:81.
19. Lal SK, Kumar P, Yeo WM, Kar-Roy A, Chow VTK. The VP1 protein of human enterovirus 71 self-associates via an interaction domain spanning amino acids 66–297. *J Viral*. 2006;78(5):582–90.
20. Huang SY, Wang Y, Yu C, Su IJ, Jen Ren Wang. Mutations in VP2 and VP1 capsid proteins increase infectivity and mouse lethality of enterovirus 71 by virus binding and RNA accumulation enhancement. *J Viral*. 2012;422(1):132–43.
21. Jiang L, Fan R, Sun S, Fan P, Su W, Zhou Y, et al. A new EV71 VP3 epitope in norovirus P particle vector displays neutralizing activity and protection in vivo in mice. *Vaccine*. 2015;33(48):6596–603.
22. Siratcha P, Jaslan D, Watee S, Jeeraphong T, Salma T, Nitat S, et al. Human Antibodies to VP4 Inhibit Replication of Enteroviruses Across Subgenotypes and Serotypes, and Enhance Host Innate Immunity. *Frontiers in Microbiology*. 2020;11:e562768.

23. Lenneke de Visser, Langereis MA, Rabouw HH, Wahedi M, Muntjewerff EM, Raoul, et al. Essential Role of Enterovirus 2A Protease in Counteracting Stress Granule Formation and the Induction of Type I Interferon. *J Viral*. 2019;93(10) e00222.
24. Wang B, Xi X, Lei X, Zhang X, Cui S, Wang J, et al. Correction: Enterovirus 71 Protease 2Apro Targets MAVS to Inhibit Anti-Viral Type I Interferon Responses. *PLOS pathogens*. 2024;20(5):e1012209.
25. Supasorn O, Tongtawe P, Srimanote P, Rattanakomol P, Thanongsaksrikul J. A nonstructural 2B protein of enterovirus A71 increases cytosolic Ca²⁺ and induces apoptosis in human neuroblastoma SH-SY5Y cells. *J Neurovirol*. 2020;26(2):201–13.
26. Westphal D, Kluck RM, Dewson G. Building blocks of the apoptotic pore: how Bax and Bak are activated and oligomerize during apoptosis. *Cell Death & Differentiation*. 2013;21(2):196–205.
27. Guan H, Tian J, Qin B, Justyna Aleksandra Wojdyla, Wang B, Zhao Z, et al. Crystal structure of 2C helicase from enterovirus 71. *Science Advances*. 2017;3(4):e1602573.
28. Xie L, Lu B, Zheng Z, Miao Y, Liu Y, Zhang Y, et al. The 3C protease of enterovirus A71 counteracts the activity of host zinc-finger antiviral protein (ZAP). *J Virol*. 2018;99(1):73–85.
29. Yi L, Lu J, Kung HF, He ML. The virology and developments toward control of human enterovirus 71. *Crit Rev Microbiol*. 2011;37(4):313–27.
30. Li X, Peng T. Strategy, Progress, and Challenges of Drug Repurposing for Efficient Antiviral Discovery. *Frontiers in Pharmacology*. 2021;12:660710.
31. Wang J, Hu Y, Zheng M. Enterovirus A71 antivirals: Past, present, and future. *Acta Pharmaceutica Sinica B*. 2022;12(4):1542–66.
32. Cox JA, Hiscox JA, Solomon T, Ooi MH, Ng LFP. Immunopathogenesis and Virus–Host Interactions of Enterovirus 71 in Patients with Hand, Foot and Mouth Disease. *Frontiers in Microbiology*. 2017;8:e2249.
33. Hellen CUT. Internal ribosome entry sites in eukaryotic mRNA molecules. *Genes & Development*. 2001;15(13):1593–612.

34. Yi L, Lu J, Kung HF, He ML. The virology and developments toward control of human enterovirus 71. *Crit Rev Microbiol*. 2011;37(4):313–27.
35. Dragovich PS, Prins TJ, Zhou R, Johnson TO, Hua Y, Luu HT, et al. Structure-based design, synthesis, and biological evaluation of irreversible human rhinovirus 3C protease inhibitors. 8. Pharmacological optimization of orally bioavailable 2-pyridone-containing peptidomimetics. *J Med Chem*. 2003;46(21):4572–85.
36. Gorbalenya AE, Donchenko AP, Blinov VM, Koonin EV. Cysteine proteases of positive strand RNA viruses and chymotrypsin-like serine proteases. *FEBS Letters*. 1989;243(2):103–14.
37. Costenaro L, Zuzanna Kaczmarek, Carme Arnan, Janowski R, Coutard B, Solà M, et al. Structural Basis for Antiviral Inhibition of the Main Protease, 3C, from Human Enterovirus 93. *J virology*. 2011;85(20):10764–73.
38. Wen W, Qi Z, Wang J. The Function and Mechanism of Enterovirus 71 (EV71) 3C Protease. *Current Microbiology*. 2020;77(9):1968–75.
39. Li X, Wang M, Cheng A, Wen X, Ou X, Mao S, et al. Enterovirus Replication Organelles and Inhibitors of Their Formation. *Frontiers in Microbiology*. 2020;11:1817.
40. Brogi S. Novel Antiviral Agents: Synthesis, Molecular Modelling Studies and Biological Investigation. *Viruses*. 2023;15(10):2042–2.
41. Ong KC, Wong KT. Understanding Enterovirus 71 Neuropathogenesis and Its Impact on Other Neurotropic Enteroviruses. *Brain Pathology*. 2015;25(5):614–24.
42. Solomon T, Lewthwaite P, Perera D, Cardoso MJ, McMinn P, Ooi MH. Virology, epidemiology, pathogenesis, and control of enterovirus 71. *The Lancet Infectious Diseases*. 2010;10(11):778–90.
43. Zhao XX, Lin FJ, Li H, Li HB, Wu DT, Geng F, et al. Recent Advances in Bioactive Compounds, Health Functions, and Safety Concerns of Onion (*Allium cepa* L.). *Frontiers in Nutrition*. 2021;8:e669805
44. Puenpa J, Wanlapakorn N, Vongpunsawad S, Poovorawan Y. The History of Enterovirus A71 Outbreaks and Molecular Epidemiology in the Asia-Pacific Region. *J Biomed Sci*. 2019;26(1):75.

45. Zheng Y, Jit M, Wu JT, Yang J, Leung K, Liao Q, et al. Economic costs and health-related quality of life for hand, foot and mouth disease (HFMD) patients in China. Larson BA, editor. PLOS ONE. 2017;12(9):e0184266.
46. Zhang Z, Liu Y, Liu F, Ren M, Nie T, Cui J, et al. Basic Reproduction Number of Enterovirus 71 and Coxsackievirus A16 and A6: Evidence From Outbreaks of Hand, Foot, and Mouth Disease in China Between 2011 and 2018. *Clinical Infectious Diseases*. 2020;73(9):2552.
47. Li R, Liu L, Mo Z, Wang X, Xia J, Liang Z, et al. An inactivated enterovirus 71 vaccine in healthy children. *N Engl J Med* 2014; 370:829.
48. Tongle Bu, Jing Li. Structure engineering of hierarchical layered perovskite interface for efficient and stable wide bandgap photovoltaics, *Nano Energy*. 2020;75:2211.
49. Zhu F, Xu W, Xia J, Liang Z, Liu Y, Zhang X, et al. Efficacy, Safety, and Immunogenicity of an Enterovirus 71 Vaccine in China. *N Engl J Med*. 2014;370(9):818–28.
50. Wang S, Pang Z, Fan H, Tong Y. Advances in anti-EV-A71 drug development research. *Journal of Advanced Research*. 2024; 56:137–56.
51. Samby K, Besson D, Dutta A, Patra B, Doy A, Glossop P, et al. The Pandemic Response Box—Accelerating Drug Discovery Efforts after Disease Outbreaks. *ACS Infectious Diseases*. 2022;8(4):713–20.
52. Tripp RA, Martin DE. Repurposing Probenecid to Inhibit SARS-CoV-2, Influenza Virus, and Respiratory Syncytial Virus (RSV) Replication. *Viruses*. 2022;14(3):612.
53. Policastro LR, Dolci I, Godoy AS, Silva Júnior JVJ, Ruiz UEA, Santos IA, et al. The Antifungal Itraconazole Is a Potent Inhibitor of Chikungunya Virus Replication. *Viruses*. 2022;14(7):1351.
- 54.. Zhang X, Song Z, Qin B, Zhang X, Chen L, Hu Y, et al. Rupintrivir is a promising candidate for treating severe cases of enterovirus-71 infection: Evaluation of antiviral efficacy in a murine infection model. *Antiviral research*. 2013;97(3):264–9.

55. Janissen R, Woodman A, Shengjuler D, Vallet T, Lee KM, Kuijpers L, et al. Induced intra- and intermolecular template switching as a therapeutic mechanism against RNA viruses. *Molecular Cell*. 2021;81(21):4467.
56. Samby K, Besson D, Dutta A, Patra B, Doy A, Glossop P, et al. The Pandemic Response Box—Accelerating Drug Discovery Efforts after Disease Outbreaks. *ACS Infectious Diseases*. 2022;8(4):713–20.
57. National Library of Medicine (US). PubChem Compound Summary for CID 406272, Pyridone-F [Internet]. PubChem. 2004 [cited 2024 June 1]. Available from: <https://pubchem.ncbi.nlm.nih.gov/compound/Pyridone-F>
58. National Library of Medicine (US). PubChem Compound Summary for CID 406272, Selinexor [Internet]. PubChem. 2004 [cited 2024 June 1] Available from: <https://pubchem.ncbi.nlm.nih.gov/compound/Selinexor>
59. National Library of Medicine (US). PubChem Compound Summary for CID 406272, (2R,3R,4S,5R)-2,3,4,5,6-pentahydroxyhexanal [Internet]. PubChem. 2004 [cited 2024 June 1]. Available from: <https://pubchem.ncbi.nlm.nih.gov/compound/167792>
60. National Library of Medicine (US). PubChem Compound Summary for CID 406272, Clemizole [Internet]. PubChem. 2004 [cited 2024 June 1]. Available from: <https://pubchem.ncbi.nlm.nih.gov/compound/Clemizole>
61. Dragovich PS, Prins TJ, Zhou R, Johnson TO, Hua Y, Luu HT, et al. Structure-based design, synthesis, and biological evaluation of irreversible human rhinovirus 3C protease inhibitors. 8. Pharmacological optimization of orally bioavailable 2-pyridone-containing peptidomimetics. *J Med Chem*. 2003;46(21):72–85.
62. Podar K, Shah J, Chari A, Richardson PG, Jagannath S. Selinexor for the treatment of multiple myeloma. *Expert Opin Pharmacother*. 2020;21(4):399–408.
63. Shirit Einav, Sobol H, Gehrig E, Glenn J. The Hepatitis C Virus (HCV) NS4B RNA Binding Inhibitor Clemizole Is Highly Synergistic with HCV Protease Inhibitors. *J Infect Dis*. 2010;202(1):65–74.

64. National Library of Medicine (US). PubChem Compound Summary for CID 406272, Danirixin [Internet]. PubChem. 2004 [cited 2024 June 1]. Available from: <https://pubchem.ncbi.nlm.nih.gov/compound/Danirixin>
65. National Library of Medicine (US). PubChem Compound Summary for CID 406272, Pocapavir [Internet]. PubChem. 2004 [cited 2024 June 1]. Available from: <https://pubchem.ncbi.nlm.nih.gov/compound/Pocapavir>
66. National Library of Medicine (US). PubChem Compound Summary for CID 406272, Plerixafor [Internet]. PubChem. 2004 [cited 2024 June 1]. Available from: <https://pubchem.ncbi.nlm.nih.gov/compound/Plerixafor>
67. Madan A, Chen S, Yates P, Washburn ML, Roberts G, Peat AJ, et al. Efficacy and Safety of Danirixin (GSK1325756) Co-administered With Standard-of-Care Antiviral (Oseltamivir): A Phase 2b, Global, Randomized Study of Adults Hospitalized With Influenza. *Open Forum Infect Dis*. 2019;6(4):163.
68. Lanko K, Sun L, Froeyen M, Leyssen P, Delang L, Mirabelli C, et al. Comparative analysis of the molecular mechanism of resistance to vapendavir across a panel of picornavirus species. *Antiviral Research*. 2021;195:e105177.
69. DiPersio JF, Uy GL, Yasothan U, Kirkpatrick P. Plerixafor. *Nature Reviews Drug Discovery*. 2009;8(2):105–7.
70. WHO Polio laboratory manual 4th edition, 2004 [Internet]. [cited 2024 June 18]. Available from: <https://iris.who.int/handle/10665/68762>
71. Wang Y, Cao L, Zhai Y, Yin Z, Sun Y, Shang L. Structure of the Enterovirus 71 3C Protease in Complex with NK-1.8k and Indications for the Development of Antienterovirus Protease Inhibitor. *Antimicrob Agents Chemother*. 2017;61(7): e00298.
72. Lei X, Sun Z, Liu X, Jin Q, He B, Wang J. Cleavage of the Adaptor Protein TRIF by Enterovirus 71 3C Inhibits Antiviral Responses Mediated by Toll-Like Receptor 3. *J Virol*. 2011;85(17):8811–8.
73. Kashyap T, Murray J, Walker CJ, Chang H, Tamir S, Hou B, et al. Selinexor, a novel selective inhibitor of nuclear export, reduces SARS-CoV-2 infection and protects the respiratory system in vivo. *Antiviral Research*. 2021;192:105115.
74. Jia X, Ganter B, Meier C. Improving properties of the nucleobase analogs T-705/T-1105 as potential antiviral. *Annu Rep Med Chem*. 2021;57:1–47.

75. Torres-Torres S, Myers AL, Klatte JM, Rhoden EE, Oberste MS, Collett MS, et al. First use of investigational antiviral drug pocapavir (v-073) for treating neonatal enteroviral sepsis. *The Pediatric Infectious Disease Journal*. 2015;34(1):52–4.
76. Epstein S, Thakkar R, Fong KT, Ng J, Bearden DR, Mishra N, et al. Compassionate-use pocapavir and immunoglobulin therapy for treatment of rituximab-associated enterovirus meningoencephalitis. *J.Neurovirol*. 2022;28(2):329–34.
77. Copelyn J, Hincks JR, Wilmschurst JM, Petersen W, Howard W, Jallow S, et al. Clearance of Immunodeficiency-associated Vaccine-derived Poliovirus Infection With Pocapavir. *Pediatr Infect Dis J*. 2020;39(5):435–7.
78. WHO Polio laboratory manual 4th edition, 2004 [Internet]. [cited 2023 June 18]. Available from: https://www.who.int/healthtopics/poliomyelitis/#tab=tab_1.
79. Vichai V, Kirtikara K. Sulforhodamine B colorimetric assay for cytotoxicity screening. *Nature Protocols*. 2006;1(3):1112–6.
80. Thanongsaksrikul J, Srimanote P, Tongtawe P, Glab-ampai K, Malik AA, Supasorn O, et al. Identification and production of mouse scFv to specific epitope of enterovirus-71 virion protein-2 (VP2). *Archives of Virology*. 2018;163(5):1141–52.
81. Pathaya R, Potjanee S, Pongsri T, Onruedee K, Oratai S, Jeeraphong T. Host neuronal PRSS3 interacts with enterovirus A71 3A protein and its role in viral replication. *Sci Reps*. 2022;12(1):e12846.
82. Podar K, Shah J, Chari A, Richardson PG, Jagannath S. Selinexor for the treatment of multiple myeloma. *Expert Opin Pharmacother*. 2020;21(4):399–408.
83. Kittisak S, Potjanee S, Pongsri T, Onruedee K, Oratai S, Pathaya R, et al. Transcriptome of human neuroblastoma SH-SY5Y cells in response to 2B protein of enterovirus-A71. *Sci reps*. 2022;12(1):e1765
84. Jia X, Ganter B, Meier C. Improving properties of the nucleobase analogs T-705/T-1105 as potential antiviral. *Annu Rep Med Chem*. 2021; 57:1–47.

85. Catching A, Ming Te Yeh, Bianco S, Capponi S, Andino R. A tradeoff between enterovirus A71 particle stability and cell entry. *Nature communications*. 2023;14(1):e7450.
86. Huang SC, Chang CL, Wang PS, Tsai Y, Liu HS. Enterovirus 71-induced autophagy detected in vitro and in vivo promotes viral replication. *J Med Virol*. 2009;81(7):1241.
87. Caspar B, Cocchiara P, Melet A, Van Emelen K, Van der Aa A, Milligan G, et al. CXCR4 as a novel target in immunology: moving away from typical antagonists. *Future Drug Discovery*. 2022;4(2): FDD77.
88. Liu N, Bauer M, Press AT. The immunological function of CXCR2 in the liver during sepsis. *J inflamm*. 2022;19(1):23.
89. Kremer KN, Peterson KL, Schneider PA, Meng XW, Dai H, Hess AD, et al. CXCR4 chemokine receptor signaling induces apoptosis in acute myeloid leukemia cells via regulation of the Bcl-2 family members Bcl-XL, Noxa, and Bak. *J Biol Chem*. 2013, 288(32):e22899-e22914.
90. Zhang H, Li F, Pan Z, Wu Z, Wang Y, Cui Y. Activation of PI3K/Akt pathway limits JNK-mediated apoptosis during EV71 infection. *Viruses*. 2014; 192:74–84.

The seal of Thammasat University is a circular emblem. It features a central five-petaled lotus flower. Above the lotus is a horizontal bar with five lines, and above that is a crown-like structure. The entire emblem is encircled by a ring containing the university's name in Thai script at the top and 'THAMMASAT UNIVERSITY' in English at the bottom, separated by two small star-like symbols.

APPENDICES

PPENDIX A

OLIGONUCLEOTIDE NUCLEOTIDE SEQUENCES

1. Primers used for detection of EV-A71 genomic RNA

Primer name 5' to 3'	sequence
EV-F2760	ATGGKTATGYWAAYTGGGACAT
EV-R3206	CCTGACRTGYTTMATCCTCAT

2. Primers used for determination of GAPDH and Beta actin using qRT PCR

Primer name	5' to 3' sequence
GAPDH-F	CAAGGTCATCCATGACAACCTTTG
GAPDH-R	GTCCACCACCCTGTTGCTGTA
Human ACTB-F	GAGCGGGAAATCGTGCGTGACATT
Human ACTB-R	GAAGGTAGTTTCGTGGATGCC

APPENDIX B

CHEMICAL REAGENTS FOR IMMUNOFLUORESCENCE

1. **4% paraformaldehyde (PFA) solution** Two grams of paraformaldehyde were dissolved in 40 mL of 1× PBS and mixed gently on magnetic stirrer hot plate. 1N NaOH was gradually added until the PFA solution became clear. Volume was filled up to 50 mL with 1× PBS. The solution was sterilized by filtration and kept as aliquots in −20 °C.

2. **0.1% Triton X-100 solution** Fifty microliters of 100% Triton X-100 were added into 50 mL of 1× PBS and mixed thoroughly using vortex. The solution was sterilized by filtration and kept at room temperature

3. **5% bovine serum albumin (BSA) solution** Bovine serum albumin (Capricorn scientific, USA) 2.5 g were dissolved in 1× PBS and mixed using vortex. The 5% BSA solution was sterilized by filtration and kept at 4 °C.

4. **1% bovine serum albumin (BSA) solution** The solution was prepared by diluting 1 in 5 of 5 % BSA in 1× PBS and kept at 4 °C.

APPENDIX C

Reagent for SDS-PAGE and western blotting

1. 6X-SDS-gel reducing loading buffer

This buffer was prepared by combining the ingredients as followed : SDS 0.6 mg, Bromophenol blue 0.5 mg, 0.5 M Tris-HCL, pH 8.8, 3.75 ml, glycerol 4.6 ml and β -mercaptoethanol 1.5 ml. The volume of the preparation was made up to 10 ml by adding UDW. The complete 6 \times sample buffer was kept in a 1 ml-aliquot at -20 °C. In SDS-PAGE one part of 6 \times sample buffer was diluted with five parts of each sample and heated at 100 °C for 5 minutes before load to the SDS-gel.

2. Washing buffer (PBS-T: 0.05% Tween-20 in 0.01 M PBS, pH 7.4)

One Liter of Phosphate buffer saline (PBS) was contained the following ingredients: 10 ml of 1 M PB, pH 7.4, 50 ml of 3 M NaCl solution and 940 ml of DW. The PBS-T was prepared by added 0.5 ml of Tween-20 to 1 liter of 0.01 M PBS, pH 7.4.

3. Ponceau S solution

0.1% (w/v) of Ponceau S ($C_{22}H_{12}N_4O_{13}S_4Na_4$) was mixed with 5% acetic acid and kept at room temperature. The colored solution was used to rapidly stain of protein bands on nitrocellulose membranes. The colored of Ponceau S is reversible by washing the membrane with DW.

4. Blocking solition (5% fetal bovine serum in PBS)

The blocking solution was prepared by added 0.5 ml of fetal bovine serum (FBS) to 10 ml of 0.01 M PBS, pH 7.4. The blocking solution was freshly prepared and use. It could not kept for long time

5. Tris Buffer (0.15 M Tris-HCl, pH 9.6)

To prepared this buffer, 18.5 g of Tris base (Amresco, PA, USA) were dissolved in 700 ml of UDW. After that the pH of Tris buffer was adjusted to 9.6 with 1 N HCl and volume was made up to 1 liter with UDW.



APPENDIX D

Reagent and buffer for Sulforhodamine B (SRB) assay

1. Sulforhodamine B sodium salt (SRB) 0.04% (w/v)

Sulforhodamine B sodium salt (SRB) (Sigma-Aldrich, MO, USA) 4 mg was dissolved in 10 ml of 1% (v/v) acetic acid by stirring. The solution was filter by wash man filter paper and kept at room temperature. Beacused this colored solution is sensitive to the light this solution must be kept avoid from light.

2. 1% Acetic acid

This solution was preared by adding 1 ml of 100% acetic acid to 99 ml of UDW. This acidic solution should prepared in glass bottle and must be prepared in fume hood with carefully practice.

3. Tris base solution 1 M, pH 10.5

Tris base (Amresco, PA, USA) 121. 14 g was dissolved in 800 ml of UDW and stirring until the chemical completely dissolved. The pH of this solution was adjusted to 10.5 with 1 N HCl and made volume up to 1 Liter with UDW.

4. Tris base solution 10 mM, pH 10.5

For 10 mM Tris base solution preparation, 10 ml of 1 M Tris base solution from (3) was diluted in 990 ml of UDW.

BIOGRAPHY

Name	Miss Nattinee Lochaiyakun
Date of birth	November 5 th , 1996
Educational Attainment	
2015-2018	Bachelor's degree of Medical Technology Faculty of Allied Health Sciences
2019-Present	Thammasat University, Thailand
Work position	Medical technology and clinic manager Navamed clinic, Pathumthani, Thailand
Scholarship (If any)	-
Publications	Novel Anti-enterovirus A71 Compounds Discovered by Repositioning Antivirals from the Open-source MMV Pandemic Response Box. Pharmaceuticals 2024 (accepted).
Work experience	<ul style="list-style-type: none"> Biology teacher (2018-2020) Alert Cadet Academy, Donmeaung, Thailand Research and Product development (2021-2022) CPRAM, Bangrak, Bkk, Thailand